



Impact of ocean warming on net primary production in the northern Indian Ocean: role of aerosols and freshening of surface ocean

B. Sridevi¹ · Sk. Sabira¹ · V.V.S.S. Sarma^{1,2}

Received: 1 August 2022 / Accepted: 14 February 2023 / Published online: 2 March 2023
© The Author(s), under exclusive licence to Springer-Verlag GmbH Germany, part of Springer Nature 2023

Abstract

Warming due to climate change stratifies the upper ocean and reduces nutrient input to the photic zone resulting in a decline in net primary production (NPP). On the other hand, climate change increases both anthropogenic aerosol input into the atmosphere and the river discharge due to the melting of glaciers on land resulting in enhanced nutrient inputs to the surface ocean and NPP. To examine the balance between these two processes, spatial and temporal variations in the rate of warming, NPP, aerosol optical depth (AOD), and sea surface salinity (SSS) were studied between 2001 and 2020 in the northern Indian Ocean. Strong heterogeneity in the warming of the sea surface was observed in the northern Indian Ocean with significant warming in the south of 12°N. Insignificant trends in warming were observed in the northern Arabian Sea (AS), north of 12°N, during winter and fall, and western Bay of Bengal (BoB) during winter, spring, and fall associated with higher levels of anthropogenic AOD (AAOD) due to a reduction in incoming solar radiation. The decline in NPP was observed in the south of 12°N in both AS and BoB and correlated inversely with SST suggesting that a weak supply of nutrients due to upper ocean stratification controlled NPP. Despite warming, the weak trends in NPP in the north of 12°N were associated with higher AAOD levels and their rate of increase suggesting that the deposition of nutrients from the aerosols seems to be compensating for declining trends due to warming. The decrease in sea surface salinity confirmed an increase in river discharge, and nutrient supply led to weak NPP trends in the northern BoB. This study suggests that the enhanced atmospheric aerosols and river discharge played a significant role in warming and changes in NPP in the northern Indian Ocean, and these parameters must be included in the ocean biogeochemical models for accurate prediction of possible changes in the upper ocean biogeochemistry in the future due to climate change.

Keywords Warming · Net primary production · Aerosols · River discharge · Climate change · Indian Ocean

Introduction

The warming due to climate change (Dong et al., 2014; Samset et al., 2018) brought significant modifications in species phenology and community composition in the marine ecosystem (Poloczanska et al., 2013; Beaugrand et al., 2013; Hoegh-Guldberg and Bruno, 2010). Several pieces of evidence on modification in the phytoplankton

community structure have been reported through numerical models and remote sensing data (Gregg and Rousseaux, 2019). Bakun, (1990) reported that global coastal upwelling may accelerate due to the intensification of alongshore wind stress that may have a dramatic impact on the marine ecosystem. A lack of long-term baseline data, and few observation time series extending back to a pre-industrial era with good spatial coverage, limits the evidence for possible long-term change in the ecosystem due to climate change (Field et al., 2006; Spielhagen et al., 2011).

The northern Indian Ocean is a unique region with reference to orography as it is bound by landmasses of South and Southeast Asia and opened to the Indian Ocean in the south. Winds change their direction with season resulting in seasonal variability in the surface currents leading to the occurrence of convective mixing and upwelling during winter and summer, respectively, in the northwestern

Responsible Editor: Philippe Garrigues

✉ V.V.S.S. Sarma
sarmav@nio.org

¹ CSIR-National Institute of Oceanography, 176 Lawsons Bay Colony, Visakhapatnam 530 017, India

² Academy of Scientific and Innovative Research (AcSIR), Ghaziabad, India

Indian Ocean (Arabian Sea (AS)) (Schott and McCreary, 2001; Fig. 1). Bakun et al., (1998) reported that coastal upwelling has a strong impact on ecosystem productivity and fish production in the western Indian Ocean. In contrast, the river discharge stratifies the water column in the northeastern Indian Ocean (Bay of Bengal (BoB)) resulting in weak coastal upwelling and an absence of convective mixing (Sarma et al., 2013, 2016). The northern Indian Ocean receives the highest amounts of anthropogenic aerosols from South and Southeast Asia (Zhang and Reid, 2010). Banerjee and Prasanna Kumar (2014) observed that episodic phytoplankton blooms in the AS are associated with dust storms. Laösher (2021) found an increase in primary production by ~30% due to the deposition of iron (Fe) through atmospheric dust in the AS suggesting that dust plays a significant role in controlling primary production.

Rapid warming of sea surface temperature (SST) in the tropical Indian Ocean was reported (Roxy et al., 2015) resulting in weak vertical transport of nutrients and a decline in primary production in the western AS during the summer monsoon (Dunstan et al., 2018; Roxy et al., 2016). A decline in Somali upwelling intensity and decreased evaporation due to the weakening of winds were attributed to the warming of the Indian Ocean in recent decades (D'Mello and Prasanna Kumar (2018). Several investigators reported both an increase and decrease in chlorophyll-a (Chl-a), a proxy for primary production, in the past few decades using different time scales of remote sensing data. For instance, a significant increase in summer monsoon phytoplankton biomass by 350% was reported in the western AS (Behrenfeld et al., 2006; Goes et al., 2005; Gregg et al., 2005) between 1998 and 2004 (7 years). It is attributed to an increase in temperature over the Eurasian landmass that enhanced the temperature gradient between land and ocean leading to an increase in summer monsoon intensity and upwelling (Goes

et al., 2005). Prakash et al., (2012) extended time-series data from 1998 to 2010 (13 years), and significant positive trends in Chl-a were observed only off Somalia during the summer (southwestern AS). Roxy et al., (2016) analyzed remote sensing data between 1997 and 2013 (16 years) and reported a significant decrease in summer Chl-a in the western AS (Off Somalia and Oman) and southeast coast of AS. In all these studies, the variability in Chl-a is studied only during summer in the AS, and its variability during other seasons and the northeastern Indian Ocean is not studied.

The long-term variability in surface Chl-a was also carried out using numerical models associated with remote sensing data. For instance, the long-term remote sensing data between 1998 and 2015 (18 years) has been assimilated to an ocean biogeochemical model and estimated a significant decline in annual primary production in the north and equatorial Indian Ocean basins (north of 10°S) associated with shallowing of the mixed layer and decrease in nutrient inputs (Gregg and Rousseaux, 2019). In these models, a significant decline in primary production was observed in the BoB and eastern AS, whereas there was an overall declining trend throughout the equatorial Indian Ocean basin rather than the more localized trends. The equatorial Indian Ocean exhibited a significant relationship between the decline in primary production and the increase in SST; however, such a relation was absent in the northern Indian Ocean (Gregg and Rousseaux, 2019). The potential mechanism responsible for the decline in primary production in the northern Indian Ocean was not evident. While remote sensing data show a decline in phytoplankton biomass in the western AS only, CMIP5 (Coupled Model Intercomparison Project) data projects a decline in the primary production in the entire AS but insignificant trends in the BoB (Bopp et al., 2013). Kong et al., (2019) observed a significant decline in modeled primary

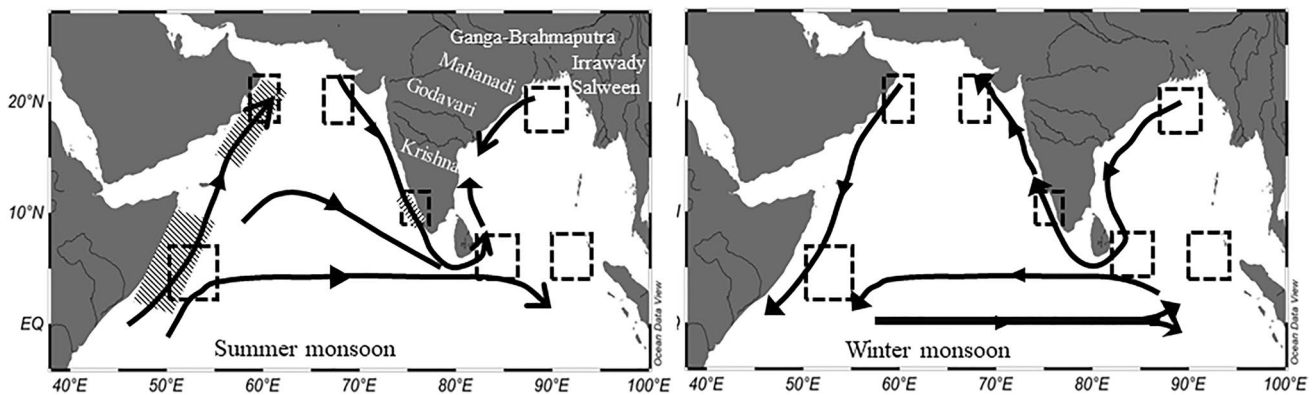


Fig. 1 The map of the study region in which the surface seasonal circulation is shown as arrows. The locations of coastal upwelling and convective mixing are identified. The major rivers discharging to the Bay of Bengal (BoB) are also shown. The region of different

zone, such as southwestern AS (SWAS), northwestern AS (NWS), northeastern AS (NEAS), southeastern AS (SEAS), northern BoB (NBoB), southwestern BoB (SWBoB), and southeastern BoB (SEBoB) are drawn

production in the BoB and the southeastern Indian Ocean during Indian Ocean Dipole (IOD) and El Niño-Southern Oscillation (ENSO) events. Therefore, a significant difference in trends in primary production was observed between models and remote sensing data and processes contributing to the spatial heterogeneity in the trends that were unclear in the northern Indian Ocean.

In remote sensing data analysis, Chl-a is used as a proxy for primary production. It is well known that the concentration of Chl-a in the phytoplankton cell responds to changes in photoacclimation, nutrient status, taxonomy, and other environmental stressors (Geider, 1987; Falkowski and La Roche, 1991; Behrenfeld et al., 2016); hence, it does not represent primary production (Westberry et al., 2008); Behrenfeld et al., 2016). The potential reasons responsible for the inconsistency between trends in warming and net primary production (NPP) and strong heterogeneity in response within the basin could not be explained (Bopp et al., 2013); Roxy et al., 2016). In addition to this, the northern Indian Ocean receives significant amounts of atmospheric aerosols from South and Southeast Asian countries, and this region is a hot spot for the production of aerosols (Ramanathan et al., 2001); Zhang and Reid, 2010). Kurokawa and Ohara, (2020) found that atmospheric pollutants are increasing rapidly in the atmosphere over South and Southeast Asia since the middle of the 1990s. Recently, Sarma et al., (2022) estimated that an increase in the aerosol mass load ($0.05\text{--}1.67\ \mu\text{g m}^{-3}\ \text{year}^{-1}$), nitrate ($0.003\text{--}0.04\ \mu\text{g m}^{-3}\ \text{year}^{-1}$), and ammonium ($0.006\text{--}0.11\ \mu\text{g m}^{-3}\ \text{year}^{-1}$) concentrations was observed between 2001 and 2020 due to an increase in anthropogenic pollutants over South and Southeast Asia. Guieu et al., (2019) estimated that atmospheric deposition of nutrients supports about 22% of the primary production in the AS, whereas Srinivas and Sarin (2013) estimated about 13% in the BoB. Recently, Sarma et al., (2022) estimated that 27–30% of the primary production is contributed by the atmospheric deposition of nutrients in the northern Indian Ocean. On the other hand, the decline in glacier over the Himalayan region was reported (Goes et al., 2020), and this resulted in an increase in river discharge to the BoB and a decrease in surface salinity (Trott et al., 2019); Sridevi and Sarma, 2021). River discharge is a source of nutrients for the BoB (Krishna et al., 2016); Sarma et al., 2019). These processes may have a significant impact on warming and NPP in the northern Indian Ocean. Hence, the objectives of this study are to (1) examine the spatial and temporal variability in surface warming in the Indian Ocean due to climate change, (2) demarcate the regions where significant modification in NPP occurred and evaluate potential reasons responsible, and (3) evaluate the role of atmospheric deposition of aerosols and freshening on changes in NPP in the northern Indian Ocean.

Material and methods

Data and methodology

Data from different sources are utilized to carry out the present work. Monthly field from linear interpolation of weekly optimum interpolation of version 2 of sea surface temperature (SST) data was obtained from the Asia-Pacific Data-Research Center (APDRC; http://apdrc.soest.hawaii.edu/dods/public_data/NOAA_SST/OISST/monthly) with a spatial resolution of $0.25^\circ \times 0.25^\circ$ during the period 2001–2020. Monthly reanalysis of sea surface salinity (SSS) data was obtained from Copernicus Marine Environment Monitoring Service (CMEMS) of GLOBAL_REANALYSIS_PHY_001_031 data product, which is a global product of monthly intervals with 0.25° spatial resolution. The detailed documentation of the product is available at <http://marine.copernicus.eu/documents/QUID/CMEMS-GLO-QUID-001-025-011-017.pdf>. The salinity data of CMEMS was compared with the satellite (Soil Moisture and Ocean Salinity (SMOS) and Soil Moisture Active Passive (SMAP)) and in situ data and found to match well (Dossa et al., 2021). Monthly Chl-a data of MODIS (Moderate Resolution Imaging Spectroradiometer) onboard Terra satellite with 9-km resolution were obtained for the period 2001 to 2020 from the Earth Observing System Data and Information System (EOSDIS; <https://giovanni.gsfc.nasa.gov/giovanni/>). Since Chl-a data from SeaWiFS (Sea-viewing Wide Field-of-view Sensor) is also available between 1997 and 2010, we compared the blended product of SeaWiFS with MODIS during the period when both data sets are available (2001–2010) and found a significant offset between these two data sets (higher MODIS than SeaWiFS) in the northern Indian Ocean. In addition to this, the difference has variability with space and time. Hence, we decided to use only the single sensor data of MODIS in this study to avoid any errors associated with differences between the two sensors. Monthly wind vector data with 0.25° spatial resolution at 10 m above the sea surface from ERA5 were used during the period 2001–2020 (http://apdrc.soest.hawaii.edu:80/dods/public_data/Reanalysis_Data/ERA5/monthly_2d/Surface). ENSO and IOD indices data were taken from <https://ggweather.com/enso/oni.htm> and https://psl.noaa.gov/gcos_wgsp/Timeseries/DMI/, respectively. Aerosol optical depth (AOD) data at 550-nm wavelength was extracted from MODIS Terra satellite (collection 6.1 and level 3) with a spatial resolution of $1^\circ \times 1^\circ$ during the period of 2001–2019, and anthropogenic (AAOD) and dust AOD (DAOD) were estimated by following Kaufman et al., (2005) as follows:

Total aerosol optical thickness (τ_p) is defined as the sum of anthropogenic (τ_{anth}) from pollution and smoke + dust

(τ_{dust}) + baseline marine (τ_{mar}) sources. Therefore, τ_f can be written as

$$\tau_f = f_{550} * \tau_{550} = (f_{\text{anth}} * \tau_{\text{anth}}) + (f_{\text{dust}} * \tau_{\text{dust}}) + (f_{\text{mar}} * \tau_{\text{mar}}) \tag{1}$$

where f_{mar} , f_{dust} , and f_{anth} are fraction fine particles from marine, dust, and anthropogenic sources. The total fine fraction (f_{550}) and optical thickness (τ_{550}) are derived from MODIS. Both τ_{dust} and τ_{anth} for the northern Indian Ocean were computed from MODIS onboard Terra using the method given by Kaufman et al. (2005) using the following equations:

$$\tau_{\text{dust}} = [f_{550}\tau_{550} - f_{\text{anth}}\tau_{\text{anth}} - f_{\text{mar}}\tau_{\text{mar}}] / -f_{\text{dust}} \tag{2}$$

By substituting Eq. 2 in Eq. 1, we get

$$\tau_{\text{anth}} = [(f_{550} - f_{\text{dust}}) - \tau_{550} - (f_{\text{mar}} - f_{\text{dust}}) * \tau_{\text{mar}}] / (f_{\text{anth}} - f_{\text{dust}}) \tag{3}$$

where τ is the monthly mean aerosol optical depth and it is a fraction of τ contributed by the fine aerosols (f) and it is obtained from MODIS/Terra from January 2001 to December 2019. f_{anth} was taken as 0.90 based on measurements in the northern Bay of Bengal (Nair et al., 2005). f_{marine} was taken as 0.47 based on measurements over the western part of the Equatorial Indian Ocean, and f_{dust} was taken as 0.32. The maritime aerosol optical depth (τ_{mar}) was obtained from the wind speed using the following equation given by Smirnov et al. (2003): $\tau_{\text{mar}} = 0.07W + 0.05$, where W is the wind speed (m/s).

Monthly NPP data were obtained from the carbon-based production model (CbPM; <http://sites.science.oregonstate.edu/ocean.productivity/index.php>) with a spatial resolution of 9 km during the period from 2001 to 2020. To bring all parameters into the same spatial resolution, both Chl-a and NPP were re-gridded to $0.25^\circ \times 0.25^\circ$ grid. Dalabehera and Sarma (2021) compared NPP by CbPM with in situ data in the Indian Ocean (north of 30°S) and found it to match within 20%.

To understand the long-term changes of all these parameters on a seasonal scale, data is prepared into seasonal means (winter, December, January, February; spring, March, April, and May; summer, June, July, August, and September; and fall, October and November), and then liner trend analysis was performed on all the parameters.

Computation of trend analysis and statistical significance

We have determined the trends and statistical significance of the parameters by following Santer et al., (2000). The trends of the parameters were computed using a least-square fit method for each seasonal data as

$$x(t) = a + bt, \text{ for } t = 1, \dots, nt$$

The significance of the computed trends was evaluated following Santer et al. (2000), in which regression residuals ($e(t)$) are defined as

$$e(t) = x(t) - xm(t); \text{ for } t = 1, \dots, nt$$

x_m is the mean value, and for statistically independent values of $e(t)$, the standard error of the slope, b , is defined as

$$Sb = Se / \left(\sum (t - tm)^2 \right)^{0.5}$$

where t_m is the mean and Se^2 is the variance of the residuals about the regression line, which is given by

$$Se^2 = (1/nt - 2) * \sum e(t)^2$$

Whether the $e(t)$ trend is significantly different from zero is tested by computing the ratio between the estimated trend and its standard error.

$$t_b = b/s_b$$

We noticed that $e(t)$ is not statistically independent; hence, autocorrelation method involving sample size is used following Santer et al., (2000).

To understand the relationship between warming and biological response, seasonal regression analysis of SST vs NPP and SST vs Chl-a was performed (Table 1). The regression analyses were performed on the seasonal mean data of each parameter in the selected boxes, such as southwestern AS (SWAS), northwestern AS (NWS), northeastern AS (NEAS), southeastern AS (SEAS), northern BoB (NBoB), southwestern BoB (SWBoB), and southeastern BoB (SEBoB) (Table 2). All the regression and trend analyses and illustrations were prepared in MATLAB.

Computation of Ekman mass transport

Using monthly wind vectors data, the Ekman mass transport (M_{xE}) was computed following bulk aerodynamic formulae based on Pond and Pickard, (1983) and Narayana et al., (2020).

$$M_{xE} = \tau_y / f \text{ where } \tau_y = \rho C_d w v;$$

where τ_y is alongshore wind stress and $\rho = 1.25$ is the density of the air (kg/m^3); C_d is drag coefficient and 1.3×10^{-3} is taken for present study; w is wind speed (m/s), v is alongshore wind (m/s), and $f = 2\omega \sin\phi$ is the Coriolis parameter (s^{-1}) for the latitude ϕ , and ω is the Earth rotation rate.

Table 1 Year-wise occurrence El Niño-Southern Oscillation (ENSO) period, IOD period with a range of index during the event from 2001 to 2020

Year	ENSO		IOD	
	Period	Index range	Period	Index range
2001				
2002	Weak El Niño; Jun–Mar	0.59–0.95		
2003				
2004	Weak El Niño; Aug–Mar	0.5–0.82		
2005				
2006	Weak El Niño; Sep–Jan	0.53–0.82	Positive; Sep–Nov	0.58–0.88
2007	Strong La Niña; Sep–Jun	–0.56 to –1.46		
2008	Weak La Niña; Nov–Feb	–0.52 to –0.72		
2009	El Niño; Aug–Apr	0.59–1.31		
2010	Strong La Niña; Jul–May	–0.53 to –1.41	Negative; Sep–Nov	–0.58 to –0.74
2011	La Niña; Aug–Mar	–0.56 to –1.04		
2012			Positive; Jul–Oct	0.41–0.89
2013				
2014	Weak El Niño; Oct–Dec	0.53–0.81		
2015	Strong El Niño; Jan–Dec–May	0.63–1.59	Positive; Jul–Nov	0.42–0.77
2016			Negative; Jun–Oct	–0.61 to –0.94
2017			Positive; Mar–Sep	0.42–0.64
2018	Weak El Niño; Sep–Dec	0.56–0.89	Positive; Aug–Nov	0.4–0.64
2019	El Niño; Jan–Dec–Apr	0.5–0.88	Positive; May–Dec	0.46–1.62
2020	La Niña; Oct–Mar	–0.5 to –0.93		

Results

Spatial variations of SST, AAOD, DAOD, SSS, Chl-a, and NPP

The SST displayed typical seasonality with cooler during winter and warmer during summer in the northern Indian Ocean. Surface waters warmed up more in the south compared to the north during all seasons in the northern Indian Ocean. In the case of BoB, the western Bay was cooler during winter than the eastern Bay and contrasted to that observed during summer and fall monsoon (Fig. 2a–d). The annual mean SST suggests that northern and western AS was cooler by $\sim 2^\circ\text{C}$ than BoB (Fig. 2f). The AAOD levels were higher along the Indian coast during all seasons (>0.3) and decreased towards the offshore region (~ 0.1). Relatively higher AAOD levels were observed during winter and fall and the least during summer (Fig. 2f–i). The annual mean AAOD suggested higher levels in the eastern AS and western BoB than in other regions in the northern Indian Ocean (Fig. 2j). Significantly higher DAOD levels were observed during summer and fall and the least during winter (Fig. 2k–o). Higher DAOD levels were observed in the AS than in BoB during all seasons. The annual mean DAOD shows higher levels in the AS, especially along the coasts of Oman, Afghanistan, Pakistan, and India, than offshore in the AS and along the east coast of India in the BoB (Fig. 2o). Significantly higher salinity was observed in the AS

compared to BoB. The lowest salinity was observed during summer and fall compared to winter and spring in the BoB with an increase in salinity from north to south (Fig. 2p–t). The annual mean salinity suggested lower salinity by 2–4 units than AS with an increase in salinity from north to south in the Bay (Fig. 2t). The concentration of Chl-a was higher in the northern AS during all seasons (Fig. 2u–y), and an increase in Chl-a was observed in the western AS during summer (Fig. 2w). The concentration of Chl-a was lower in the Bay with less seasonality (Fig. 2u–x). The annual mean Chl-a was higher in the western and northern AS than in BoB (Fig. 2y). The NPP was higher in the western AS during all seasons with a peak during fall and winter, whereas it was higher during fall and summer in the BoB. NPP increased from north to south in the BoB, whereas it decreased from west to east in the AS (Fig. 2z–cc). The annual mean NPP was higher in the AS than in BoB with an increase in NPP from north to south in the Bay (Fig. 2dd).

During the study period, the Indian Ocean experienced several atmospheric extreme events such as El Niño (with strong, moderate, and weak), La Niña, and Indian Ocean Dipole (IOD), except for 4 years (2001, 2003, 2005, and 2013). The summary of ocean-atmospheric coupled events, the period of their occurrence, and the climatic index (DMI, ENSO) are given in Table 1. The strong El Niño occurred in 2009, 2015, and 2019, whereas positive IOD was noticed in 2006, 2012, 2015, 2017 to 2019. Most of these events occurred during the fall and winter

Table 2 The mean rate of seasonal change in properties in the selected boxes in the northern Indian Ocean. The significance of rates is given as *, **, ***, **** for $p \leq 0.1$, $p < 0.05$, $p < 0.01$, and $p < 0.001$, respectively

Region	Parameter	Winter	Spring	Summer	Fall	Annual
SWAS 53–58°E and 2–7°N	SST	*0.030	***0.033	**0.037	****0.059	****0.038
	SSS	0.0123	−0.0119	−0.0024	0.0031	−0.0016
	Chl	−0.0021	0.0002	*−0.0117	**−0.0036	−0.0039
	AAOD	***0.0038	***0.0033	***−0.0023	***0.0040	**0.0016
	DAOD	−0.0002	0.0005	**0.0033	0.0006	*0.0016
	NPP	*−10.5	*−5.2	−5.8	**−11.4	*−8.0
NWA 58–61°E and 18–22°N	SST	−0.002	0.017	**0.031	0.007	0.016
	SSS	−0.0014	0.0032	0.0006	0.0046	0.0018
	Chl	−0.0118	−0.0147	−0.0542	−0.0190	−0.0209
	AAOD	**0.0023	0.0019	−0.0037	****0.0082	0.0011
	DAOD	0.0010	0.0025	**0.0174	*0.0070	**0.0108
	NPP	1.9	*−5.0	1.3	−1.8	−1.9
NEAS 66–69°E and 18–22°N	SST	0.004	**0.032	**0.041	0.021	***0.027
	SSS	0.0016	0.0066	0.0046	0.0026	0.0030
	Chl	−0.0080	0.0058	−0.0141	0.0017	−0.0036
	AAOD	****0.0087	***0.0033	−0.0016	****0.0160	***0.0041
	DAOD	0.0011	0.0037	*0.0119	*0.0040	**0.0105
	NPP	−0.13	−2.0	−6.1	−6.1	−5.2
SEAS 75–78°E and 9–12°N	SST	0.0153	**0.0366	**0.0341	*0.0239	***0.0292
	SSS	0.0202	−0.0049	−0.0047	−0.0141	−0.0017
	Chl	−0.0032	−0.0105	0.0091	−0.0030	−0.0026
	AAOD	****0.0172	****0.0173	−0.0013	***0.0165	****0.0105
	DAOD	0.0005	−0.0015	*0.0053	0.0025	**0.0046
	NPP	1.1	−1.0	**−13.9	**−7.2	−8.4
NBoB 87–91°E and 17–21°N	SST	0.0010	*0.0146	****0.0496	*0.0113	***0.0246
	SSS	**−0.0413	*−0.0195	***−0.028	**−0.0263	***−0.0265
	Chl	0.0037	−0.0012	0.0007	0.0034	0.0018
	AAOD	****0.0189	****0.0168	**0.0064	***0.0151	****0.0129
	DAOD	0.0000	−0.0003	−0.0016	0.0008	−0.0007
	NPP	5.9	−6.0	5.9	6.2	1.4
SEBoB 90–94°E and 4–8°N	SST	**0.0200	***0.0360	**0.0229	***0.0322	****0.0273
	SSS	−0.0011	−0.0084	−0.0024	−0.0122	−0.0054
	Chl	0.0022	0.0006	0.0006	0.0002	0.0005
	AAOD	−0.0006	0.0021	−0.0016	0.0026	0.0003
	DAOD	−0.0003	−0.0002	**0.0039	0.0004	*0.0019
	NPP	3.9	−0.7	−3.9	*−5.4	*−4.0
SWBoB 82–86°E and 4–8°N	SST	*0.0237	**0.0318	*0.0145	**0.0272	***0.0233
	SSS	0.0042	0.0016	−0.0032	−0.0173	−0.0033
	Chl	0.0006	0.0001	0.0019	−0.0001	0.0005
	AAOD	0.0022	0.0027	−0.0016	*0.0039	0.0012
	DAOD	−0.0001	0.0005	**0.0036	0.0002	*0.0020
	NPP	−0.01	***−1.4	−0.76	***−6.7	**−3.7

seasons. The supplementary figures S1 present the time-series variations in SST, SSS, DAOD, AAOD, and NPP in the selected boxes and identified the major climatic events. Slight warming of sea surface temperature and insignificant variations in Chl-a and NPP was observed during El Niño and IOD than normal periods (Fig. S1).

Spatial variations of SST trends

The spatial distribution of trends in SST between 2001 and 2020 indicated strong heterogeneity during all seasons in the northern Indian Ocean (Fig. 3a–d). Significant warming was confined to the south of 12°N in the AS and BoB

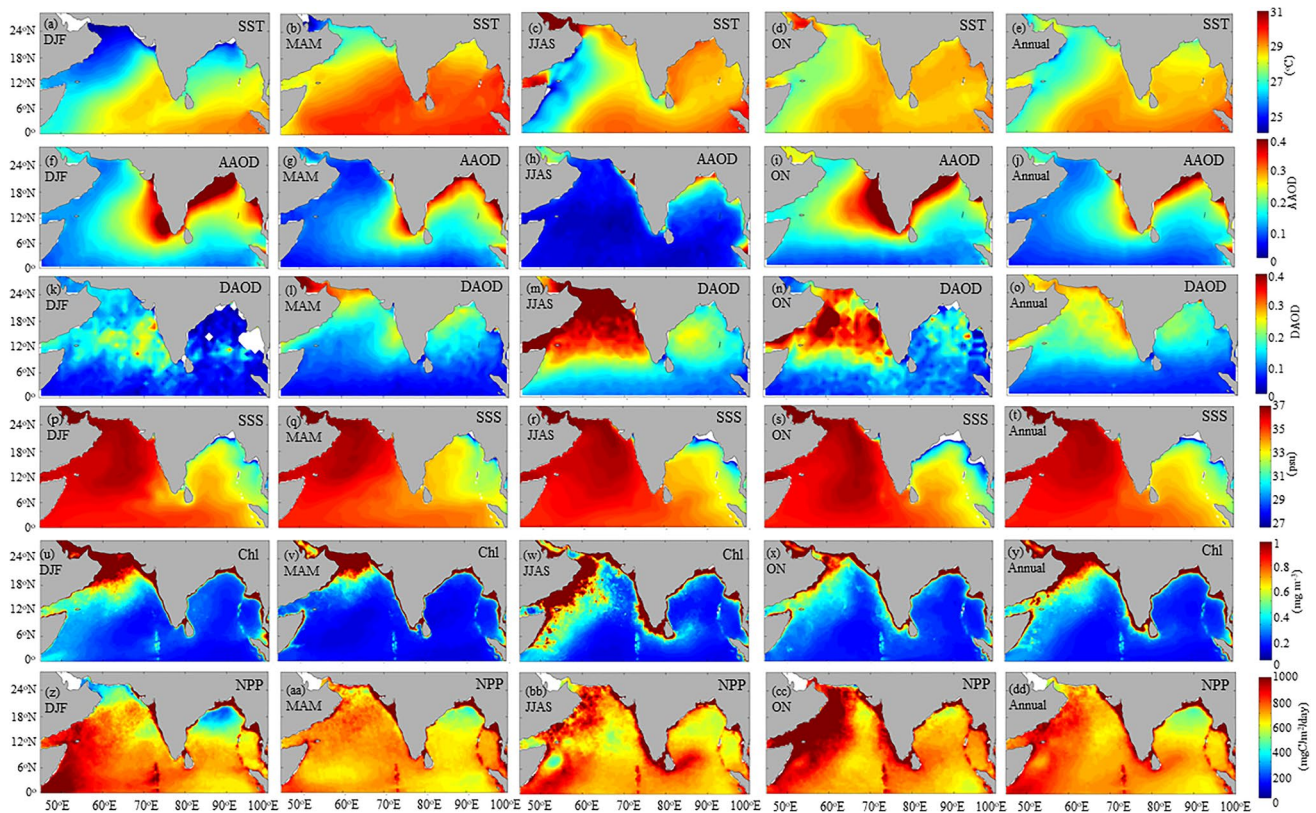


Fig. 2 Seasonal mean climatology of sea surface temperature (SST) during (a) winter (DJF), (b) spring (MAM), (c) summer (JJAS), (d) fall (ON) monsoon and (e) annual mean, AAOD (f–j), DAOD (k–o),

salinity (p–t), chlorophyll-a (Chl-a) (mg m^{-3} ; u–y), and net primary production (NPP) ($\text{mgC m}^{-2} \text{day}^{-1}$; z–dd) in the northern Indian Ocean

during winter, whereas slight cooling was observed in the northern basins (north of 12°N). But the cooling trends were statistically not significant at 90% confidence levels. The warming of the entire northern Indian Ocean was observed during summer, except for the south-central Indian Ocean, with a relatively higher rate of warming in the western and northern AS and northern BoB ($0.05^\circ\text{C}/\text{year}$) compared to the southern basin ($0.02^\circ\text{C}/\text{year}$; Fig. 3a–d). Higher warming was observed in the southwestern AS ($0.05^\circ\text{C}/\text{year}$) during fall and insignificant warming in the northern BoB and central AS (Fig. 3d). The northern and western BoB displayed an insignificant warming during winter, spring, and fall monsoons. The eastern BoB (Andaman Sea) was warmed during all seasons with a higher rate during spring ($0.04^\circ\text{C}/\text{year}$) and fall ($0.03^\circ\text{C}/\text{year}$) than in other seasons. The annual mean trends in SST suggest significant warming of the entire northern Indian Ocean at a rate of $\sim 0.03^\circ\text{C}/\text{year}$ at a 90% confidence interval with relatively higher warming in the western AS and eastern BoB with insignificant trends in the northwestern and southeastern regions of the northern Indian Ocean (Fig. 3e).

Spatial variations of AAOD and DAOD trends

The AAOD displayed a significant positive trend in the AS during winter, spring, and fall monsoons with a higher rate of increase in the eastern than western basin (Fig. 3f–i). Significant decreasing trends in AAOD were observed during summer in the entire AS (Fig. 3h). The rate of increase in AAOD was higher during fall followed by winter along the east coast of AS (Fig. 3f, i). In the case of BoB, significant positive trends in AAOD were observed along the west coast of BoB during all seasons with a higher rate during winter followed by spring and fall (Fig. 3f, i). Insignificant trends in AAOD were observed in the south and southeastern BoB, including the Andaman Sea, during all seasons. The weak cooling or insignificant warming trends were observed along the western BoB associated with higher AAOD during all seasons (Fig. 3a–i). The annual mean trends in AAOD suggest an increase in AAOD in the northern Indian Ocean with a higher rate of increase in the eastern AS and western BoB, whereas insignificant trends were noticed in the northwestern AS and southeastern BoB (Fig. 3j). The DAOD

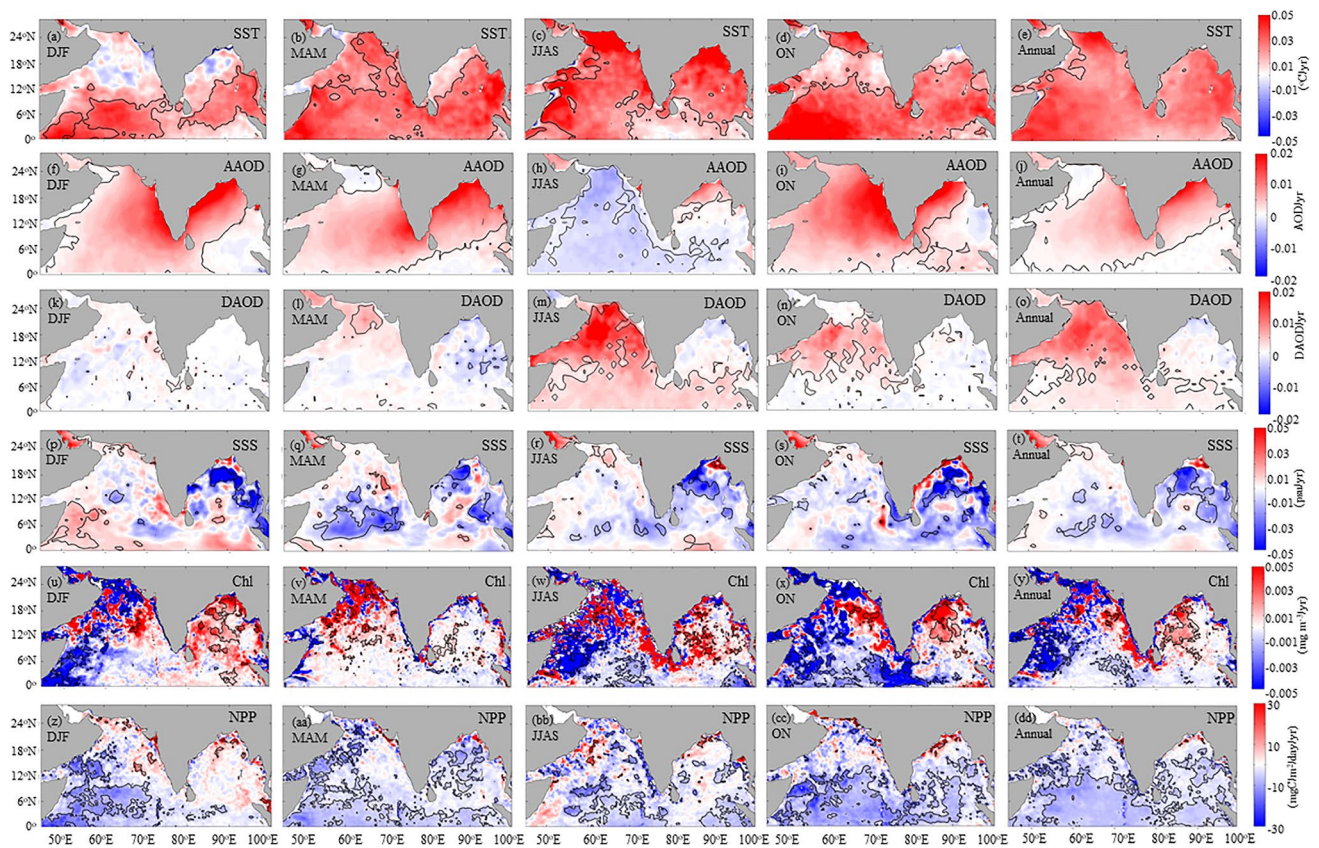


Fig. 3 The seasonal trends in SST during (a) winter (DJF), (b) spring (MAM), (c) summer (JJAS), (d) fall (ON) monsoon and (e) annual mean, AAOD (f–j), DAOD (k–o), salinity (p–t), Chl-a (mg m^{-3} ; u–

y), and NPP ($\text{mg C m}^{-2} \text{ day}^{-1}$; z–dd) in the northern Indian Ocean. The thick black contour line in the figures indicates significance at a >90% confidence level

displayed significant increasing trends during summer in the entire AS and southern BoB and central AS during the fall monsoon season (Fig. 3m, n). The insignificant trends were observed during winter, spring in the northern Indian Ocean, and fall monsoon in the BoB. The spatial distribution of seasonal SST displayed an inverse relation with AAOD during winter ($r^2=0.84$; $p<0.001$) and spring ($r^2=0.59$; $p<0.001$), and it is insignificant during summer and fall (Supplementary Figure S2). The DAOD did not display significant relation with SST in the northern Indian Ocean.

Spatial variations of SSS trends

The SSS displayed patchy trends with reference to space and time in the northern Indian Ocean. Significant decreasing trends were observed during all seasons in the northern and central BoB and the Andaman Sea (Fig. 3p–s). The declining trends in SSS were confined to northwestern BoB during spring and summer whereas the entire northern and central BoB during winter and fall monsoon seasons. Especially declining trends in SSS were observed along the coastal region, and it was stronger during the fall monsoon (Fig. 3s).

Insignificant trends in SSS were observed in the AS during summer and fall but increasing trends in the southwestern AS during winter and declining trends in the southern AS during spring were observed (Fig. 3p, q). The annual mean trend suggested that salinity decreased in the BoB, especially north of 10°N , whereas insignificant trends were noticed in the AS (Fig. 3t).

Spatial variations of Chl-a trends

The rate of change in Chl-a exhibited strong heterogeneity in the northern Indian Ocean. Significant decreasing trends were observed off Somalia in the southwestern AS during the winter, summer, and fall monsoons (Fig. 3u–x). Though a positive trend in Chl-a was observed in the northern AS during spring, it was not significant at a 90% confidence level. Positive trends in Chl-a were observed in the northern BoB during winter and fall monsoon (Fig. 3u, x). Despite positive trends in Chl-a were observed off Oman, the southeast coast of AS, and western BoB during summer, they are not statistically significant at 90% confidence levels. The annual mean trends in Chl-a suggested a decreasing trend in

the AS, whereas a significant increasing trend was observed in the western BoB (Fig. 3y). Chl-a displayed significant inverse relation with SST in the southern and central AS during winter and western AS during spring, southwestern and central AS during summer, and southern AS during fall monsoon seasons (Fig 4a–d). Though trends in Chl-a were significant only in a few regions in the AS, the relationship between Chl-a and SST suggested the significant impact of warming on Chl-a in the entire basin in the AS. In the case of BoB, a significant inverse relation between SST and Chl-a was observed in the western BoB during winter and southern (south of 6°N) BoB during fall monsoon (Fig. 4a and d).

Spatial variations of NPP trends

The overall declining trends in NPP were observed in the northern Indian Ocean with large spatial variability. Significant declining trends in NPP were observed in the southern AS and BoB during all seasons, except during winter in the BoB. The area covered with a decline in NPP was more during spring and fall monsoons than in other seasons (Fig. 3z–cc). The declining trends in NPP were observed off Somalia in southwestern AS during all seasons, and it was relatively weaker during summer and stronger during fall and winter. A significant decline in NPP was observed in the northwestern AS during spring, and it was insignificant during other seasons. No significant trends in NPP were observed in the eastern AS. A significant decline in NPP was observed during spring in the entire AS, whereas it was only in the southern BoB during fall (Fig. 3)cc. The annual mean trends in NPP suggested a decrease in the south of 12°N in the northern Indian Ocean and insignificant trends in the north of 12°N (Fig. 3)dd. The declining trends in NPP were consistent with the warming trends in the northern Indian Ocean. The SST and NPP displayed a significant inverse correlation in the southern AS (south of 12°N) during winter and fall and southwestern AS during spring and summer

(Fig. 4e–h). In the case of BoB, this relationship was significant only during the fall monsoon in the SWBoB (Fig. 4h).

Regional variability of trends in SST, SSS, Chl-a, and NPP

To examine the regional variability in trends of SST, SSS, Chl-a, and NPP, the northern Indian Ocean is divided into 7 regions, as shown in Fig. 1, and the mean rate of changes was given in Table 2. SST displayed a significant warming trend during all seasons (0.030 to 0.059°C year⁻¹) in the SWAS with an annual mean rate of 0.038°C year⁻¹ associated with an insignificant trend in salinity and declining trends in Chl-a (−0.0036, −0.0117 mg m⁻³ year⁻¹) during fall and summer and NPP (−11.4 to −5.2 mgC m⁻² day⁻¹ year⁻¹) during all seasons. Significant positive trends in AAOD were observed during all seasons (0.0019 to 0.0189 year⁻¹) in the AS and NBoB, except during summer whereas summer and spring seasons in the NWAS region (Table 2). Insignificant trends in AAOD were observed in the SWBoB and SEBoB. DAOD displayed a significant positive trend during summer (0.0033 year⁻¹), but it was insignificant during other seasons at SWAS (Table 2). In the case of the NWAS, significant warming was observed only during summer (0.031°C year⁻¹), whereas insignificant changes were observed during other seasons with annual insignificant warming (Fig. 3a–f; Table 2). AAOD exhibited a positive trend during the winter and fall seasons (0.0023 to 0.0082 year⁻¹) in the NWAS. DAOD displayed a positive trend during the summer and fall seasons only (Fig. 3m, n) with an annual rate of increase of 0.0108 year⁻¹. Insignificant variability in surface salinity and Chl was observed during any season at a 90% confidence interval (Fig. 3p–y). The significant decreasing trend in NPP was observed only during spring (−5.0 mgC m⁻² day⁻¹ year⁻¹) in the NWAS, whereas it was insignificant during other seasons. Significant

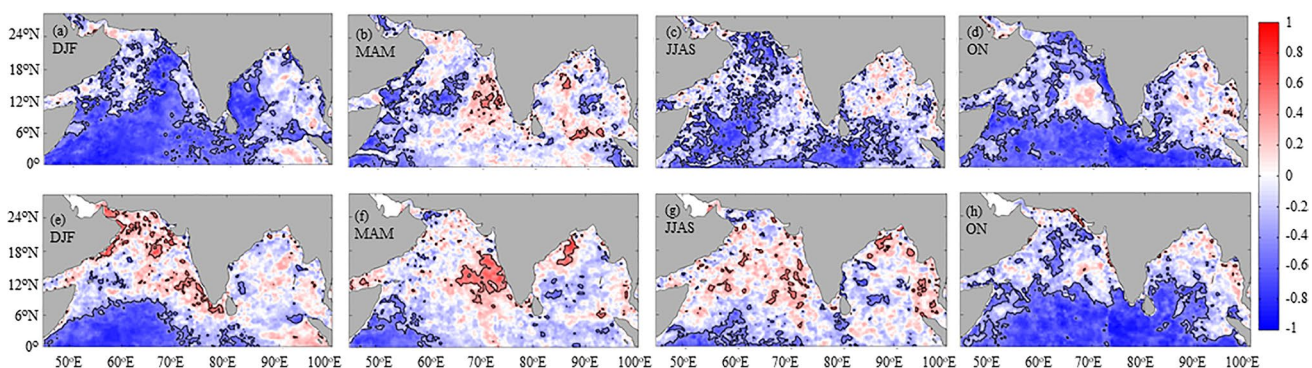


Fig. 4 The relationship between SST and Chl-a during (a) winter (DJF), (b) spring (MAM), (c) summer (JJAS), and fall (ON) monsoon and the same with NPP (e–h). The thick black contour line in the figures indicates significance at a >90% confidence level

warming of SST was observed only during spring and summer (0.032 and $0.041^{\circ}\text{C year}^{-1}$) with an annual mean rate of $0.027^{\circ}\text{C year}^{-1}$ associated with positive trends in AAOD during all seasons, except summer in the NEAS. DAOD displayed a significant positive trend during summer and fall (Table 2). Both Chl-a and NPP did not display significant trends in the NEAS. Warming trends were observed during all seasons (0.024 to $0.037^{\circ}\text{C year}^{-1}$), except winter, associated with insignificant trends in salinity and Chl-a in the SEAS. A significant positive trend in AAOD (0.0165 to 0.0173 year^{-1}) was observed during all seasons except summer in the SEAS. An increasing trend in DAOD was significant only during summer. Chl-a did not display a significant trend, whereas the decline in NPP was observed during summer and fall (-7.2 to $-13.9 \text{ mgC m}^{-2} \text{ day}^{-1} \text{ year}^{-1}$) in the SEAS.

In the NBoB, significant warming was observed during all seasons (0.0113 to $0.0496^{\circ}\text{C year}^{-1}$), except winter, associated with a significant positive trend in AAOD during all seasons (0.006 to 0.0189 year^{-1}). Insignificant trends in DAOD, Chl-a, and NPP were found (Table 2). A significant decline in salinity was observed during all seasons (-0.019 to 0.041 year^{-1}) in the NBoB. NPP did not display significant trends in the NBoB. Significant warming trends in the sea surface were observed during all seasons (0.0145 – $0.0318^{\circ}\text{C year}^{-1}$) with annual mean warming of $0.0233^{\circ}\text{C year}^{-1}$ with insignificant trends in SSS, and Chl-a was observed in the SWBoB. AAOD exhibited a positive trend during fall whereas DAOD during summer in the SWBoB. NPP displayed a declining trend during the spring and fall seasons (-1.4 and $-6.7 \text{ mgC m}^{-2} \text{ day}^{-1} \text{ year}^{-1}$) in the SWBoB. Significant warming was observed during all seasons (0.020 to $0.036^{\circ}\text{C year}^{-1}$), and no significant trends in SSS, Chl-a, and AAOD were observed in the SEBoB. DAOD displayed a positive trend during summer, and a decline in NPP was observed during fall ($-5.4 \text{ mgC m}^{-2} \text{ day}^{-1} \text{ year}^{-1}$) in the SEBoB.

The peak in the rate of warming exhibited seasonal variability with reference to space as a peak in spring/fall monsoon was observed in the south of 12°N [SWAS ($0.059^{\circ}\text{C year}^{-1}$), SEAS ($0.0366^{\circ}\text{C year}^{-1}$), SWBoB ($0.0318^{\circ}\text{C year}^{-1}$), and SEBoB ($0.036^{\circ}\text{C year}^{-1}$)], whereas it was during summer in the north of 12°N [Nwas ($0.031^{\circ}\text{C year}^{-1}$), NEAS ($0.041^{\circ}\text{C year}^{-1}$), and NBoB ($0.049^{\circ}\text{C year}^{-1}$)]. Similarly, the peak in a season of a significant declining trend in NPP also displayed spatial variability with a higher declining trend during fall monsoon in the south of 12°N [SWAS ($-11.4 \text{ mgC m}^{-2} \text{ day}^{-1} \text{ year}^{-1}$), SEAS ($-13.9 \text{ mgC m}^{-2} \text{ day}^{-1} \text{ year}^{-1}$), SWBoB ($-6.7 \text{ mgC m}^{-2} \text{ day}^{-1} \text{ year}^{-1}$), and SEBoB ($-5.4 \text{ mgC m}^{-2} \text{ day}^{-1} \text{ year}^{-1}$)], whereas it was during spring in the north of 12°N [Nwas ($-5.0 \text{ mgC m}^{-2} \text{ day}^{-1} \text{ year}^{-1}$) and NBoB ($-6.9 \text{ mgC m}^{-2} \text{ day}^{-1} \text{ year}^{-1}$)] (Table 2).

Discussion

Heterogeneity in warming trends in the northern Indian Ocean

The warming between 2001 and 2020 during summer in the western AS is almost double ($\sim 0.03/\text{year}$) than that reported between 1950 and 2012 ($\sim 0.016^{\circ}\text{C}/\text{year}$; Roxy et al., 2016) (Table 2). The rate of warming displayed a significant seasonal and spatial variability with slight cooling or insignificant warming observed in the north of 12°N in the northern Indian Ocean during the winter, spring, and fall monsoon periods. The patchy warming trends in the northern Indian Ocean may be caused by local processes than global warming.

The Indian Ocean receives anthropogenic aerosols during winter associated with northeasterly winds and mineral dust and sea salt during summer with southwesterly winds (Li and Ramanathan, 2002). The major source of dust in the northern Indian Ocean comes from the Nubian Desert, the Arabian Peninsula, Iran, Pakistan, Afghanistan, and North-West India with maximum activity between May and October (Pease et al., 1998; Leon and Legrand, 2003). Higher DAOD levels and positive trends (0.01 to $0.02/\text{year}$) were observed during summer and fall (Fig. 3m, n) over the AS, but their trends were insignificant in the BoB. In contrast, the trends in AAOD were higher along with the western coastal BoB ($>0.01/\text{year}$) and eastern coastal AS during all seasons, except summer in the AS (Fig. 3f–i). A higher rate of increase in AAOD over the northern Indian Ocean was reported over the past two decades (Zhang and Reid, 2010; Yadav et al., 2021). Distribution and trends of both AAOD and DAOD were higher in the north of 12°N than south of the northern Indian Ocean (Fig. 3f–o), whereas higher warming trends were observed in the south of 12°N than north (Fig. 3a–d) suggesting the significant impact of aerosols on heterogeneity in warming trends.

The higher positive SST trends were observed during summer in the AS than in other seasons associated with higher levels and positive trends of DAOD (Fig. 3m) and lower levels and negative trends of AAOD (Fig. 3h) suggesting a significant role of AAOD in controlling SST trends in the northern Indian Ocean. Similarly, weaker or insignificant trends in SST were found in the western BoB (Fig. 3a–d) during all seasons, except summer, associated with higher positive AAOD (Fig. 3f–i) and insignificant DAOD trends (Fig. 3k–n) further confirming that AAOD plays a significant role on the warming of northern Indian Ocean. Ramanathan et al., (2001) suggested that Indo-Asian aerosols, called Asian Brown Clouds (ABC), have a significant impact on radiative forcing through cooling (-20 W m^{-2}) at the surface and comparable heating of the

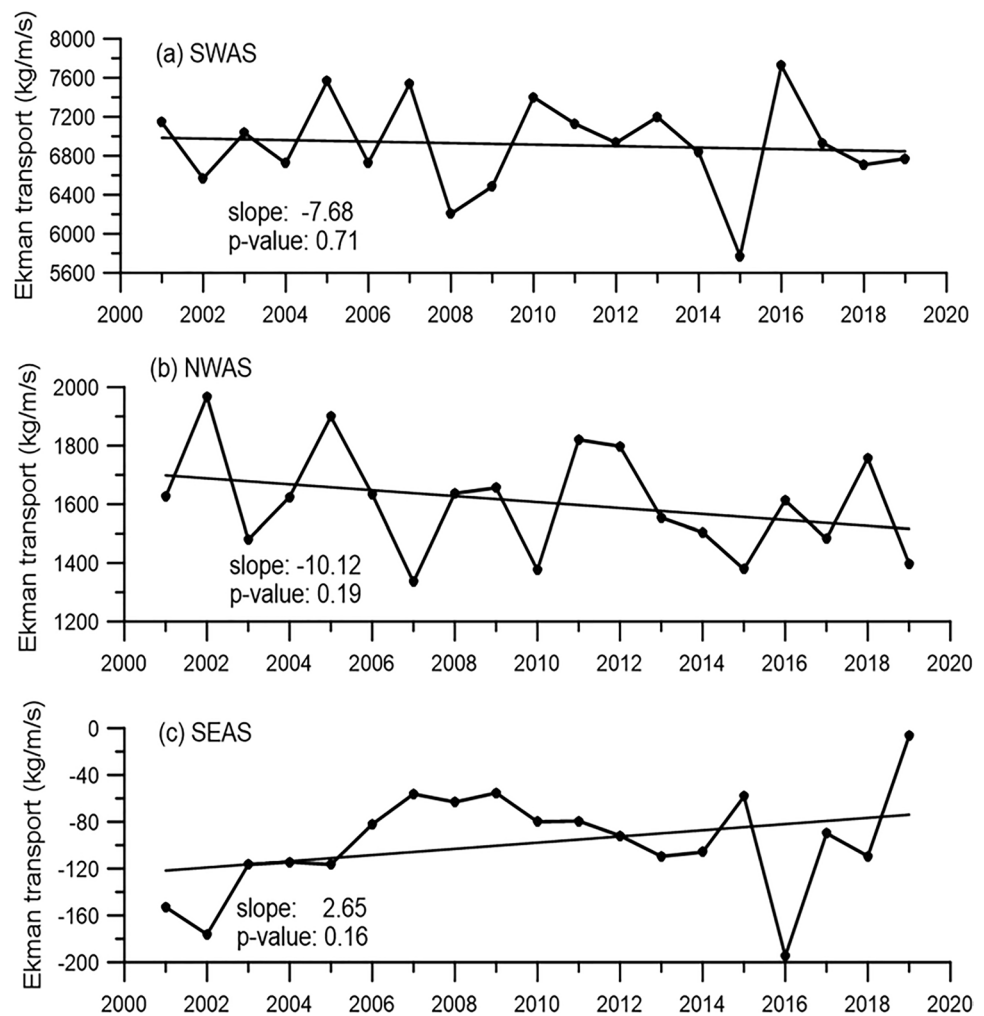
atmosphere at higher altitudes. Sarma et al., (2015) found that cooling of 1.3°C between 1991 and 2011 during winter and spring seasons in the northwestern BoB attributed to enhanced loading of anthropogenic aerosols. The fraction of AAOD to the total AOD was higher during winter and spring (60–70%) than in summer (30–40%) over the Indian Ocean (Satheesh and Srinivasan, 2002), and therefore, it lowers more incoming solar radiation during former than later seasons. AAOD displayed a significant inverse relation with SST in the BoB during winter ($r^2=0.84$; $p<0.001$) and spring ($r^2=0.59$; $p<0.001$), and this relationship is insignificant during summer (Supplementary figure S2). Dong et al., (2014) reported that the cooling of SST due to aerosols is more significant over the BoB than AS due to higher levels of AAOD in the former region. Zhu et al., (2007) also noticed a decrease in radiative forcing associated with dust plumes in the global ocean. Therefore, the heterogeneity in the SST warming trend in the northern Indian Ocean may be mainly caused by the inhibition of incoming solar radiation due to anthropogenic aerosols.

In addition to this, the significant warming in the SWAS and NWAS during summer may also be contributed to

variations in the strength of winds and upwelling (Table 2). To examine this, the upwelling index was computed in the selected region in the SWAS, NWAS, and SEAS regions where seasonal upwelling occurs during summer (Barber et al., 2001); Gupta et al., 2021). The Ekman mass transport suggested that a significant decreasing trend between 2001 and 2020 in SWAS, NWAS, and SEAS regions (Fig. 5) indicate that the weakening of upwelling decreased the injection of cooler subsurface waters leading to warming. D’Mello and Prasanna Kumar, (2018) also suggested that warming off Somalia and Oman’s coasts were caused by a decrease in upwelling and evaporation, respectively. Based on global circulation models, deCastro et al., (2016) observed that upwelling intensity may be increased under the RCP 8.5 scenario in the north of 8.5°N off Somalia coast, and it is contrasting to that of long-term trends based on remote sensing data (D’Mello and Prasanna Kumar, 2018); Roxy et al., 2016); present study.

On the other hand, AAOD levels and their trends were restricted to north and western coastal BoB, and insignificant trends were found in the open sea region during the

Fig. 5 Long-term variability in Ekman mass transport (upwelling index; kg/m/s) during summer at **a** SWAS, **b** NWAS, and **c** SEAS regions



summer and fall monsoon seasons (Fig. 3h, i). But the warming trends were observed in the entire BoB during summer and fall monsoon (Fig. 3c, d) irrespective of AAOD trends suggesting that other than AAOD may be contributed to the warming. The decreasing trends in SSS were observed during all seasons in the northern and central Bay, but it was spread to the entire Bay during the summer and fall monsoon seasons between 2001 and 2020 (Fig. 3r–s). Similar trends were reported between 1993 and 2014 in the northern and central BoB (Kumar et al., 2016); Trott et al., 2019). Since Ganga-Brahmaputra riverine system originates in the Himalayan mountains, where the precipitation accumulates in the form of snow and it is the source of freshwater to the Bay. Due to the rise in atmospheric temperature (IPCC, 2013; Lozan et al., 2001), Goes et al., (2020) reported a significant decline in ice cover over the Himalayan mountains over the past three decades that might have contributed to an increase in river discharge and a decrease in SSS in the BoB (Kumar et al., 2016); Paul, 2018); Trott et al., 2019; Sridevi and Sarma, 2021). The increase in riverine freshwater influx stratifies the upper water column leading to the warming of the entire BoB during the summer and fall monsoon seasons (Fig. 3c, d). Therefore, the heterogeneity in SST warming trends in the northern Indian Ocean was contributed by trends in anthropogenic aerosols and sea surface salinity.

Heterogeneity NPP in response to warming in the northern Indian Ocean

The present study suggests an ~40% decline in Chl-a in southwestern AS during the summer and fall monsoon seasons between 2001 and 2020, and it was higher than the earlier study of 20% between 1950 and 2012 (Roxy et al., 2016). The difference in decline in Chl-a between 1950–2012 and 2001–2020 may be associated with the warming trend. Significant declining trends in Chl-a were reported only in the western AS during the summer between 1998 and 2013 with insignificant trends in the eastern AS and BoB (Roxy et al., 2016). In contrast, the declining trends in NPP were observed in the entire southern AS and BoB during all seasons (Fig. 3z–cc), where insignificant trends in Chl-a were observed (Fig. 3u–x). The trends in NPP were contrasted to that of Chl-a in some regions in the northern Indian Ocean. For instance, significant declining trends in Chl-a were observed in SWAS during summer ($-0.0117 \text{ mg m}^{-3} \text{ year}^{-1}$; Fig. 3u) associated with insignificant declining trends in NPP (Fig. 3z). In contrast, insignificant trends in Chl-a were observed during spring in the southwestern AS (Fig. 4q) associated with a significant declining trend in NPP (Fig. 3)aa. On the annual scale, the decline in NPP was observed in the south of 12°N and insignificant trends

in the north of 12°N in the northern Indian Ocean (Fig. 3) dd. In contrast, a significant decline in Chl-a was observed in southwestern AS and an increasing trend in the western BoB whereas insignificant trends in the other regions (Fig. 3y). This study suggests that Chl-a trends do not represent NPP trends in the northern Indian Ocean.

In general, trends in surface Chl do not translate into trends in NPP because of varying Chl: C ratios (Behrenfeld et al., 2016); Westberry et al., 2008) or subsurface production (Cullen, 1982); Winn et al., 1995); Behrenfeld et al., 2005) Nevertheless, this study suggests that significant decline in primary production occurs in the northern Indian Ocean, south of 12°N , during all seasons at the rate of 10 to $15 \text{ mgC m}^{-2} \text{ day}^{-1} \text{ year}^{-1}$, whereas the impact was lower in the north of 12°N , except during spring monsoon (Fig 3z–cc). This is consistent with a higher rate of warming in the south of 12°N than north of 12°N in the northern Indian Ocean (Fig. 3a–d). The significant inverse relationship between SST and NPP was observed in the south of 12°N in the AS during winter and both AS and BoB during fall, whereas it was restricted to SWAS during spring and summer (Fig. 4e–h). This suggested that the decline in NPP in the other regions may be contributed by other than warming in the northern Indian Ocean. Similarly, SST also displayed a significant inverse relationship with Chl-a (Fig. 4a–d) in the AS during all seasons suggesting that warming of the upper ocean decreased the standing stock of phytoplankton due to a decrease in nutrient input. Nevertheless, the influence of warming on Chl-a was found in most of the regions in the AS compared to that of NPP as an increase in SST; therefore, solar radiation may affect fluorescence quenching leading to a decrease in NPP. In contrast, the relationship between SST and Chl-a was weaker in the BoB, where warming was relatively lower (0.0113 to $0.0496^\circ\text{C}/\text{year}$) compared to that of AS (0.0239 to $0.059^\circ\text{C}/\text{year}$), which may probably result in less impact on Chl-a changes in the former basin.

The declining trend in NPP co-occurred with warming, consistent with a shut-off of nutrients in the south of 12°N . On the other hand, despite significant warming occurring in the NBoB during summer, the NPP trends were insignificant (Fig. 3z–cc). In addition, cooling or insignificant warming occurred in the western BoB during all seasons, except summer (Fig. 3c), and northern AS during winter and fall (Fig. 3a and d) where insignificant trends in NPP were observed suggesting that other than warming may be responsible for the weak response of NPP in the north of 12°N in the northern Indian Ocean. As discussed above, with the strong role of aerosols and the freshening of surface waters on the warming of the upper ocean, it is possible that the heterogeneity in NPP may also be caused by them in the northern Indian Ocean.

Role of aerosols on weakening of NPP trends in the northern Indian Ocean

Insignificant trends in SST (or slight cooling) and NPP during winter, spring, and fall in the western BoB and northern AS (north of 12°N) during winter and fall monsoon were associated with higher levels and positive trends in AAOD and DAOD than in other regions (Fig. 3f–i, k–n). The higher DAOD levels and positive trends during summer and fall (Fig. 3m, n) suggest a significant contribution of Fe and phosphorus to the northern AS through mineral dust. In contrast, insignificant trends in DAOD were noticed in the BoB, except southern bay during summer, (Fig. 3m) indicating weak transport of Fe and phosphorus to the BoB. Chinni et al. (2019) observed that dissolved Fe concentrations were above 0.6 nM in the BoB, and it may not limit primary production (Morel et al., 1991); Schoffman et al., 2016). In contrast, the rate of increase in AAOD was higher along with the western coastal BoB (>0.01/year) and eastern coastal AS during all seasons, except summer in the AS (Fig. 3f–i) suggesting the contribution of nitrogen nutrients to the northern Indian Ocean. A higher rate of increase in AAOD over the northern Indian Ocean was reported over the past two decades (Zhang and Reid, 2010); Yadav et al., 2021). Distribution and trends of both DAOD and AAOD were higher in the north of 12°N than south in the northern Indian Ocean suggesting that a significant amount of Fe, phosphorus, and nitrogen may be deposited over the northern Indian Ocean (north of 12°N) increasing Chl-a and NPP.

Several studies revealed that atmospheric aerosols are a strong source of nutrients, especially Fe and phosphorus (dust), nitrogen (anthropogenic aerosols) nutrients, to the surface ocean that supports primary production (Duce et al., 2008; Mahowald et al., 2011; Boyd et al., 2010). An increase in phytoplankton biomass associated with dust storms was reported in the northern Indian Ocean (Banerjee and Prasanna Kumar, 2014; Patra et al., 2007; Prasanna Kumar et al., 2010; Shafeeque et al., 2017). Guieu et al. (2019) found that atmospheric dust deposition including Fe and only N and P enhanced NPP by 30 and 3%, respectively, suggesting that Fe input by dust is an important controlling factor of NPP in the AS. Enhanced primary production by 3 to 33% in the BoB was reported due to dry deposition of atmospheric nitrogen and <5% in the AS (Srinivas et al., 2011; Srinivas and Sarin 2013; Yadav et al., 2016; Bikkina et al., 2021), whereas Sarma et al. (2022) reported 27–30% of the primary production in the northern Indian Ocean supported by atmospheric aerosols. Variable rate of increase in DAOD and AAOD in the north of 12°N than south of the northern Indian Ocean suggests that increased NPP due to Fe and nitrogen deposition may be compensated for the decrease due to warming. It is further observed that Fe contribution by dust and nitrogen by anthropogenic aerosols

contributed dominantly to the increase in NPP in the AS, whereas anthropogenic aerosol contribution is significant in the BoB.

Role of river discharge on weakening of NPP trends in the BoB

Significant decreasing trends in the SSS have been observed during all seasons in the Bay suggesting freshening of the upper layer (Fig. 3p–s). Freshwater is a significant source of nutrients (both organic and inorganic) to the BoB and supports primary production (Gauns et al., 2005; Sarma et al., 2019). The decreasing trends in SSS between 2001 and 2020 in the northern and central Bay suggest that a significant amount of nutrients may be entered into the Bay through river discharge that might have compensated for nutrient decrease through vertical mixing due to warming. Therefore, this study suggests that an increase in nutrients through river discharge and atmospheric deposition may be responsible to compensate for the decrease in NPP caused by warming resulting in negligible trends in NPP in the northern and western BoB and northern AS. The enhanced nitrogen supply through rivers and dry deposition of atmospheric aerosols modify N/P ratios in the upper ocean that change phytoplankton composition and food web dynamics (Yadav et al., 2016; Kumari et al., 2022). Continuous monitoring of these sensitive zones is highly essential to examine possible changes in ecosystem structure in the future.

Regional variability in decline in NPP in the northern Indian Ocean

The trends in warming and decline in NPP displayed significant regional variability. The peak in warming was observed during summer in the north at 12°N whereas the fall monsoon in the south at 12°N in the AS and BoB suggesting that the northern basin is warmed earlier than the south. On the other hand, a peak in decline in NPP was observed in the north of 12°N during spring, whereas it was fall monsoon in the south of 12°N in the AS and BoB. The peak in warming and decline in NPP were consistent with each other in the south of 12°N in the AS and BoB but not in the north suggesting that other than warming is controlling the decline in NPP in the former region.

Though annual mean warming is not significantly different in the AS (0.025°C/year) than BoB (0.022°C/year), the annual mean rate of decline in NPP was higher in the AS, with more decline in the SWAS (~7%) followed by NWS and SEAS (~4.5%), than BoB (2.5–3.2%) indicating that warming alone is not responsible for the decline in the NPP in the northern Indian Ocean. On the other hand, the annual mean AAOD over the AS is lower (0.134±0.07) than BoB (0.156±0.06) suggesting that more anthropogenic pollutants

reach the BoB than AS, and it is consistent with the earlier reports (Srinivas and Sarin, 2013). The chemical composition of aerosols suggests that more concentrations of nitrate were observed in the aerosols over the BoB than in the AS (Kumar et al., 2008). In contrast, the annual mean DAOD is higher in the AS (0.28) than in BoB (0.19) suggesting that mineral dust brought more Fe to the former region than in the latter. Therefore, the lower rate of decline NPP in the BoB and AS may be contributed by the deposition of nutrients (Fe, N, P) from the atmosphere in the northern basin (north of 12°N). The higher decline in NPP in the SWAS, NWAS, and SEAS regions compared to other regions in the northern Indian Ocean is caused by a decrease in Ekman mass transport due to a decrease in winds (Fig. 5; Roxy et al., 2016; D'Mello and Prasanna Kumar, 2018). On the other hand, enhanced nutrients (especially nitrate and phosphate) associated with Chl-a were simulated in the NBoB (Roxy et al., 2016), and it is contrasting with the present results. Due to the use of historical river discharge data or lack of real-time river discharge data, models could not be able to capture the real contribution of nutrient supply by rivers to the BoB. In addition, the chemical composition of the river water, mainly the Ganges and Brahmaputra, is unknown to incorporate in the model. Similarly, the atmospheric source of nutrients is also not part of most of the models to account for its impact on primary production. Recently Sarma et al. (2022) estimated monthly mean inorganic nitrogen concentrations in the aerosols using AOD in the northern Indian Ocean. Therefore, the inclusion of these processes in the models would highly improve the prediction of possible changes in NPP and the ecosystem in the future due to climate change.

To examine the major controlling factors on NPP in the northern Indian Ocean, multiple linear regression (MLR) analysis was conducted with NPP as a dependent variable and others as independent (Table 3). The NPP in the selected regions (Fig. 1) displayed significant seasonal variability. For instance, the decrease in NPP was observed during all seasons in the SWAS, only during spring in the NWAS and summer/fall in the SEAS. Similarly, a decrease in NPP was noticed in the selected region during spring and summer in the NBoB, SWBoB, and SEBoB (Fig. 3z–dd). Based on the MLR analysis, the decrease in NPP was contributed by a decrease in the intensity of upwelling, as evidenced by a decrease in Ekman mass transport (Fig. 5), and during summer, warming of SST leads to a decrease in nutrient inputs during spring and fall. The increase in NPP was noticed due to an increase in DAOD and AAOD during winter and summer in the SWAS (Table 3). The declining trends in NPP during spring in the NWAS and SEAS during the fall monsoon were contributed by the warming of the sea surface leading to a decrease in nutrient inputs to the photic zone. The increase in NPP was contributed by the increase

in aerosol inputs during spring and summer in the NWAS, NEAS, and SEAS. The significant decline in NPP during the summer and fall monsoons in the NBoB, SEBoB, and SWBoB was mainly contributed by warming and a decrease in salinity, whereas an increase in NPP due to an increase in aerosols was noticed during winter and summer. In summary, the south of 12°N was influenced by warming and a decrease in upwelling intensity, whereas salinity decreased and the input of nutrients through aerosols modified NPP in the north of 12°N.

Summary and implications to biogeochemistry of Northern Indian Ocean

To examine the impact of the warming on NPP in the northern Indian Ocean, two decades of long data were analyzed. It was noticed that strong heterogeneity in warming of the sea surface trends was observed in the northern Indian Ocean with significant warming in the south of 12°N but weaker in the north of 12°N associated with higher AOD in the former than the latter region. The enhanced AOD decreased incoming solar radiation resulting in weaker warming in the north of 12°N in the northern Indian Ocean. A significant decrease in NPP was observed in the south of 12°N in both AS and BoB and inversely correlated with SST suggesting the weak supply of nutrients. Either weak or no trends in NPP in the north of 12°N were associated with higher dust and anthropogenic AOD levels, and their rate of increase suggests that the deposition of iron and nutrients from the aerosols seems to be compensating for declining trends due to warming. A significant decrease in sea surface salinity was observed in the northern BoB suggesting that an increase in river discharge and nutrient supply might have supported NPP to compensate decrease due to warming, resulting in weak trends in the northern BoB.

Climate change is rapidly warming the surface ocean in the northern Indian Ocean; however, the warming is not uniform due to higher levels of atmospheric aerosols. Though a significant decline in NPP was observed in the northern Indian Ocean, it is weaker in the northern regions where the intense oxygen minimum zone (OMZ) occurs. The occurrence of strong OMZ was reported in the northeastern AS (Sarma et al., 2020a) and northwestern BoB (Udaya Bhaskar et al., 2021). A significant warming was observed above the OMZ regions only during summer with an insignificant change observed during other seasons (Table 2). The annual NPP declined in the northeastern AS by 22%, whereas it was 10% in the northern BoB. As a result, the sinking carbon fluxes to the OMZ are expected to be declined resulting in a weakening of OMZ. In contrast, the expansion of OMZ was reported through numerical modeling due to the warming

Table 3 The multiple regression coefficients and their significance values during different seasons in the selected regions. n.s. represents not significant

Region	Season	SST		SSS		Chla		AAOD		DAOD	
		Coeff	<i>p</i> -value	Coeff	<i>p</i> -value	Coeff	<i>p</i> -value	Coeff	<i>p</i> -value	Coeff	<i>p</i> -value
SWAS	Winter	23.3	n.s	−49.5	n.s	2055.9	<0.001	−792.6	<0.01	2.7	<0.001
	Spring	−28.2	<0.05	70.3	n.s	1131.5	<0.01	74.5	n.s	0.3	n.s
	Summer	7.9	n.s	45.1	n.s	545.1	<0.001	−257.5	n.s	−1638.6	<0.001
	Fall	−29.0	n.s	67.4	n.s	2012.3	<0.001	−319.5	n.s	−0.3	n.s
	Annual	−38.3	<0.05	62.7	n.s	632.3	<0.001	564.2	<0.01	−0.5	n.s
NWAS	Winter	135.9	<0.001	−168.9	n.s	−184.6	<0.001	−176.7	n.s	0.9	n.s
	Spring	−8.0	n.s	327.6	n.s	−42.0	n.s	−1461.1	n.s	−1029.5	<0.01
	Summer	1.3	n.s	−395.1	n.s	0.9	n.s	292.0	<0.05	−292.2	<0.05
	Fall	−101.8	n.s	−609.4	n.s	132.8	<0.1	433.1	n.s	1.5	n.s
	Annual	56.3	<0.001	−655.8	n.s	−0.6	n.s	−1.3	n.s	2.2	<0.001
NEAS	Winter	15.5	n.s	−31.6	n.s	−189.5	<0.05	−422.4	n.s	0.0	n.s
	Spring	−40.5	<0.1	154.8	<0.1	−36.0	n.s	−1216.7	<0.05	−1058.2	<0.001
	Summer	−1.1	n.s	73.8	n.s	−16.3	n.s	645.1	n.s	47.3	<0.01
	Fall	6.5	n.s	−20.1	n.s	765.9	<0.01	−402.7	n.s	−0.1	n.s
	Annual	−9.6	n.s	−34.8	n.s	0.2	n.s	0.0	n.s	−0.4	n.s
SEAS	Winter	97.0	<0.1	47.5	<0.05	987.8	<0.001	−252.2	<0.05	0.1	n.s
	Spring	38.3	n.s	32.5	n.s	255.4	<0.1	−52.0	n.s	0.0	n.s
	Summer	−18.1	n.s	138.6	n.s	−4.1	n.s	2163.1	<0.05	−264.6	<0.01
	Fall	−181.3	<0.05	16.6	n.s	183.7	<0.001	−139.9	n.s	−0.2	n.s
	Annual	−24.8	n.s	121.2	<0.001	−2.9	n.s	43.6	n.s	−0.6	n.s
NBoB	Winter	20.9	n.s	59.2	n.s	1177.0	<0.01	308.0	n.s	−1.0	<0.1
	Spring	29.1	n.s	−59.1	n.s	548.4	n.s	−225.8	n.s	0.6	n.s
	Summer	70.2	<0.05	−25.3	<0.01	−0.3	n.s	−302.9	<0.1	−360.3	<0.01
	Fall	53.2	n.s	15.6	n.s	380.5	n.s	107.9	n.s	−1.5	n.s
	Annual	34.7	<0.001	−21.3	<0.001	−1.2	n.s	−24.4	n.s	−0.5	<0.1
SEBoB	Winter	51.6	<0.05	3.7	n.s	1798.0	<0.001	−698.8	<0.05	0.2	n.s
	Spring	−5.7	n.s	17.5	n.s	1584.8	<0.001	196.0	n.s	−0.3	n.s
	Summer	13.2	n.s	−53.3	<0.05	529.1	<0.5	98.0	n.s	−271.0	<0.1
	Fall	−50.0	<0.05	0.2	n.s	1670.0	<0.01	−96.4	n.s	−1236.6	<0.05
	Annual	6.4	n.s	−10.0	n.s	1261.6	<0.001	−0.2	n.s	0.2	n.s
SWBoB	Winter	18.8	n.s	44.9	<0.1	659.8	<0.01	−582.2	<0.05	0.4	n.s
	Spring	−35.8	<0.05	−9.6	n.s	1294.8	<0.05	24.7	n.s	0.0	n.s
	Summer	31.2	n.s	40.3	<0.01	545.9	<0.001	−238.0	n.s	−892.1	<0.001
	Fall	−85.2	<0.01	84.7	<0.001	1253.8	<0.001	−292.2	<0.05	0.4	n.s
	Annual	−2.7	n.s	89.4	<0.001	678.4	<0.001	0.0	n.s	0.0	n.s

of the upper ocean by 10% per decade in the northern AS (Lachkar et al., 2019). They further reported that the upper ocean warming and stratification are very sensitive to the transport of oxygen to the OMZ, and it is the main reason for the expansion of OMZ in the AS. In contrast, our study suggests that warming is not uniform in the northern AS due to the reduction of incoming solar radiation by atmospheric aerosols. In addition to this, the decline in the NPP reduces sinking carbon flux leading to a decrease in the microbial oxygen demand resulting in an increase in oxygen in the OMZ. Though warming is expected to decrease

oxygen levels, a decrease in sinking carbon fluxes and subsequent decomposition may compensate for oxygen levels in the OMZ in the northern Indian Ocean. Several global models suggested that OMZ is stable over the past several decades in the northern Indian Ocean (Oschlies et al., 2018; Stramma et al., 2008; Breitburg et al., 2018). The long-term unsystematic time-series data analysis suggests a decline in oxygen in the OMZ between 15 and 20°N by 0.09 to 0.18 $\mu\text{M}/\text{year}$ and an increase in oxygen in the north of 20°N in the AS (Banse et al., 2014). On the other hand, the CMIP5 models projected the intensification and expansion of OMZ

in the northern Indian Ocean due to climate change (Bopp et al., 2013). The recent model comparison (Coupled Model Intercomparison Project Phase 6; CMIP6) with the higher horizontal resolution, complex biogeochemical models, and improved representation of O₂ in the OMZ showed that a rate of deoxygenation in the 100–600-m layer is up to 40% faster than in the CMIP5-based projections (Seferian et al., 2020; Kwiatkowski et al., 2020).

The deposition of atmospheric aerosols seems to be promoting primary production in the northern Indian Ocean (Patra et al., 2007; Guieu et al., 2019; Srinivas and Sarin 2013). The chemical composition of atmospheric aerosols suggests higher concentrations of dissolved inorganic and organic nitrogen, whereas phosphate is very low. The deposition of atmospheric nitrogen enhances the N:P ratios in the upper ocean. This may lead to a severe limitation of phosphate in the upper ocean. Recently, Sarma et al. (2020b) observed a severe limitation of phosphate in the BoB to primary production and nitrogen fixation (Sarma et al., 2020c). The removal of phosphate through adsorption on suspended particles was observed in the BoB resulting in severe limitations (Rao et al., 2021). Under a business-as-usual scenario, the increase in atmospheric aerosols may deposit more amount of nitrogen on the surface ocean of the BoB and removes phosphate from the water column through adsorption (Rao et al., 2021), which may lead to severe limitation of phosphate in the BoB in future.

Roxy et al. (2016) indicated that the decline in primary production might have contributed to some extent to a rapid decline in the tuna fish caught in the Indian Ocean. They also observed an increase in tuna catch in some regions associated with a decline in Chl-a concentration suggesting complexity in the food web controlled by various other processes. Nevertheless, this study suggests that insignificant changes in NPP occurred along the coastal regions in the northern Indian Ocean, where the maximum fish catch is being obtained, indicating that the decline in fish catch may not be contributed by the availability of prey (phytoplankton) but may be possible due to warming. On the other hand, significant warming along the Indian coast is observed only during summer, whereas it is insignificant in most parts of coastal India during other seasons suggesting that warming also may not be a potential reason for the decline in fish catch. The other potential reasons such as migration to other regions due to several unknown physicochemical factors must be evaluated to understand the reason behind the decline in the fish caught along the Indian coast.

Nevertheless, this study suggests that atmospheric aerosols have a significant impact on the biogeochemistry of the northern Indian Ocean. None of the numerical models, neither global nor regional, include the impact of atmospheric aerosols and their impact on ocean warming and biogeochemistry in the northern Indian Ocean. Though

atmospheric aerosols influence may not be very important in the global ocean, its impact cannot be ignored in the northern Indian Ocean with reference to warming and nutrients inputs (Dong et al., 2014; Srinivas et al., 2011; Yadav et al., 2016) and ocean acidification (Doney et al., 2007; Sarma et al., 2015) due to unique orographic settings and faster industrial development along the coastal regions surrounded by the northern Indian Ocean. Since a significant amount of data is available, through observations and satellites, it would be interesting to include the impact of atmospheric pollution on the biogeochemistry of the northern Indian Ocean in the models to simulate the impact of climate change on carbon and nitrogen cycling in the future.

Supplementary Information The online version contains supplementary material available at <https://doi.org/10.1007/s11356-023-26001-9>.

Acknowledgements We would like to thank the teams of MODIS, model outcomes of CMEMS, and carbon-based primary production for making it available for this study. We would like to thank the two anonymous reviewers for their constructive criticism on the earlier version of the manuscript which improved the presentation of our results. SS has conducted this work as a part of her M.Tech dissertation, submitted to Jawaharlal Nehru Technological University (JNTU), Kakinada, and would like to thank the Head of the Department, JNTU, and the Director, CSIR-NIO for their support and encouragement to conduct this work. This has the NIO contribution number.....

Author's Contribution BS: processing of data, preparation of figures, and contribution to preparing the initial draft of the manuscript

SB: downloading data, processing data, and contributing to preparing the manuscript

VVSS: concept of the work, guidance, and finalizing of the manuscript

Data Availability The data used in this study is derived from publicly available websites, and the same information is given in the "Material and methods" section. The processed data are available upon request to the corresponding author by email (sarmav@nio.org).

Declarations

Ethics approval and consent to participate Not applicable

Consent for publication All authors are agreed to publish. No consent is required from others.

Competing interests The authors declare no competing interests

References

- Bakun A (1990) Global climate change and intensification of coastal upwelling. *Science* 247:198–201. <https://doi.org/10.1126/science.247.4939.198>
- Bakun A, Roy C, Lluch-Cota S (1998) Coastal upwelling and other processes regulating ecosystem productivity and fish production in the western Indian Ocean: large marine ecosystems of the Indian Ocean: Assessment, sustainability, and management. Blackwell Science. Malden MA (USA) 1998:103–141

- Banerjee P, Prasanna Kumar S (2014) Dust-induced episodic phytoplankton blooms in the Arabian Sea during winter monsoon. *J. Geophys. Res. Oceans* 119:7123–7138
- Banse K, Naqvi SWA, Narvekar PV, Postel JR, Jayakumar DA (2014) Oxygen minimum zone of the open Arabian Sea: variability of oxygen and nitrite from daily to decadal time scales. *Biogeosciences* 11:2237–2261
- Barber RT, Marra J, Bidigare RC, Codispoti LA, Halpern D, Johnson Z, Latasa M, Goericke R, Smith SL (2001) Primary productivity and its regulation in the Arabian Sea during 1995. *Deep Sea Res. Part II* 48:1127–1172
- Beaugrand G, McQuatters-Gollop A, Edwards M, Goberville E (2013) Long-term responses of North Atlantic calcifying plankton to climate change. *Nat. Clim change* 3:263–267
- Behrenfeld MJ, O'Malley RT, Siegel DA, McClain CR, Sarmiento JL, Feldman GC, Milligan AJ, Falkowski PG, Letelier RM, Boss ES (2006) Climate-driven trends in contemporary ocean productivity. *Nature* 444(7120):752–755
- Behrenfeld MJ, Boss E, Siegel DA, Shea DM (2005) Carbon-based ocean productivity and phytoplankton physiology from space. *Glob. Biogeochem* 19(1)
- Behrenfeld MJ, O'Malley RT, Boss ES, Westberry TK, Graff JR, Halsey KH, Milligan AJ, Siegel DA, Brown MB (2016) Reevaluating ocean warming impacts on global phytoplankton. *Nat. Clim. Change* 6(3):323–330
- Bikkina P, Sarma VVSS, Kawamura K, Srinivas B (2021) Dry-deposition of inorganic and organic nitrogen aerosols to the Arabian Sea: sources, transport and biogeochemical significance in surface water. *Mar. Chem* 231:103938
- Bopp L, Resplandy L, Orr JC, Doney SC, Dunne JP, Gehlen M, Halloran P, Heinze C, Ilyina T, Seferian R, Tjiputra J (2013) Multiple stressors of ocean ecosystems in the 21st century: projections with CMIP5 models. *Biogeosciences* 10(10):6225–6245
- Boyd PW, Mackie DS, Hunter KA (2010) Aerosol iron deposition to the surface ocean—modes of iron supply and biological responses. *Mar. Chem* 120(1–4):128–143
- Breitbart D, Levin LA, Oschlies A, Grégoire M, Chavez FP, Conley DJ, Garçon V, Gilbert D, Gutiérrez D, Isensee K, Jacinto GS (2018) Declining oxygen in the global ocean and coastal waters. *Science* 359(6371):eaam7240
- Cullen JJ (1982) The deep chlorophyll maximum: comparing vertical profiles of chlorophyll a. *Can. J. Fish. Aquat* 39(5):791–803
- Dalabehera HB, Sarma VVSS (2021) Physical forcing controls spatial variability in primary production in the Indian Ocean. *Deep-Sea Res II*(83):104906
- deCastro M, Sousa MC, Santos F, Dias JM, Gomez-Gesteira M (2016) How will Somali coastal upwelling evolve under future warming scenarios? *Sci. Res. Nat* 6:30137. <https://doi.org/10.1038/srep30137>
- D'Mello JR, Prasanna Kumar S (2018) Processes controlling the accelerated warming of the Arabian Sea. *Int J Climatol* 38(2):1074–1086
- Doney Scott C, Mahowald N, Lima I, Feely RA, Mackenzie FT, Lamarque J-F, Rasch PJ (2007) Impact of anthropogenic atmospheric nitrogen and sulfur deposition on ocean acidification and the inorganic carbon system. *Proc Natl Acad Sci U S A* 104:14580–14585
- Dong L, Zhou T (2014) The Indian Ocean Sea surface temperature warming simulated by CMIP5 models during the twentieth century: competing forcing roles of GHGs and anthropogenic aerosols. *J. Clim* 27(9):3348–3362
- Dossa AN, Alory G, da Silva AC, Dahunsi AM, Bertrand A (2021) Global analysis of coastal gradients of sea surface salinity. *Remote Sens* 13:2507. <https://doi.org/10.3390/rs13132507>
- Duce RA, LaRoche J, Altieri K, Arrigo KR, Baker AR, Capone DG, Cornell S, Dentener F, Galloway J, Ganeshram RS, Geider RJ (2008) Impacts of atmospheric anthropogenic nitrogen on the open ocean. *Science* 320(5878):893–897
- Dunstan PK, Foster SD, King E, Risbey J, O'Kane TJ, Monselesan D, Hobday AJ, Hartog JR, Thompson PA (2018) Global patterns of change and variation in sea surface temperature and chlorophyll a. *Sci. Rep* 8(1):1–9
- Falkowski PG, LaRoche J (1991) Acclimation to spectral irradiance in algae. *J. Phycol* 27(1):8–14
- Field DB, Baumgartner TR, Charles CD, Ferreira-Bartrina V, Ohman MD (2006) Planktonic foraminifera of the California Current reflect 20th-century warming. *Science* 311:63–66
- Geider RJ (1987) Light and temperature dependence of the carbon to chlorophyll a ratio in microalgae and cyanobacteria: implications for physiology and growth of phytoplankton. *New Phytol* 106:1–34
- Goes JI, Thoppil PG, Helga do R, Gomes J, Fasullo T (2005) Warming of the Eurasian landmass is making the Arabian Sea more productive. *Science* 308(5721):545–547
- Goes JI, Tian H, do Rosario Gomes H, Anderson OR, Al-Hashmi K, DeRada S, Luo H, Al-Kharusi L, Al-Azri A, Martinson DG (2020) ecosystem state change in the Arabian Sea fuelled by the recent loss of snow over the Himalayan-tibetan plateau region. *Sci. Rep* 10(1):1–8
- Gregg WW, Rousseaux CS (2019) Global Ocean primary production trends in the modern ocean color satellite record (1998–2015). *Environ. Res. Lett* 14(12):124011
- Gregg WW, Casey NW, McClain CR (2005) Recent trends in global ocean chlorophyll. *Geophys. Res. Lett* 32(3)
- Guieu C, Al Azhar M, Aumont O, Mahowald N, Levy M, Ethe C, Lachkar Z (2019) Major impact of dust deposition on the productivity of the Arabian Sea. *Geophys. Res. Lett* 46:6736–6744
- Gupta GVM, Jyothibabu R, Ramu CV, Reddy AY, Balachandran KK, Sudheesh V, KumarS CNVHK, Bepari KF, Marathe PH, Reddy BB (2021) The world's largest coastal deoxygenation zone is not anthropogenically driven. *Env Res. Lett* 16:054009
- Hoegh-Guldberg O, Bruno JF (2010) The impact of climate change on the world's marine ecosystems. *Science* 328(5985):1523–1528
- IPCC (2013) In: Stocker TF, Qin D, Plattner GK, Tignor M, Allen SK, Boschung J, Nauels A, Xia Y, Bex V, Midgley PM (eds) *Climate Change 2013: The Physical Science Basis. Contribution of Working Group I to the Fifth Assessment Report of the Intergovernmental Panel on Climate Change*. Cambridge University Press, Cambridge, United Kingdom and New York, NY, USA
- Kaufman YJ, Boucher O, Tanré D, Chin M, Remer LA, Takemura T (2005) Aerosol anthropogenic component estimated from satellite data. *Geophys. Res* 32(17)
- Kong F, Dong Q, Xiang K, Yin Z, Li Y, Liu J (2019) Spatiotemporal variability of remote sensing ocean net primary production and major forcing factors in the tropical eastern Indian and Western Pacific Ocean. *Remote Sens* 11(4):391
- Krishna MS, Prasad MHK, Rao DB, Viswanadham R, Sarma VVSS, Reddy NPC (2016) Export of dissolved inorganic nutrients to the northern Indian Ocean from the Indian monsoonal rivers during discharge period. *Geochim. Cosmochim. Acta* 172:430–443
- Kumar A, Sudheer AK, Sarin MM (2008) Chemical characteristics of aerosols in MABL of Bay of Bengal and Arabian Sea during spring inter-monsoon: a comparative study. *J. Earth Syst. Sci* 117(1):325–332
- Kumar PD, Paul YS, Muraleedharan KR, Murty VSN, Preenu PN (2016) Comparison of long-term variability of sea surface temperature in the Arabian Sea and Bay of Bengal. *Reg. Stud. Mar. Sci* 3:67–75
- Kumari VR, Neeraja B, Rao DN, Ghosh VRD, Rajula GR, Sarma VVSS (2022) Impact of atmospheric dry deposition of nutrients on phytoplankton pigment composition and primary production in the coastal Bay of Bengal. *Environ. Sci. Pollut. Res* 29(54):82218–82231. <https://doi.org/10.1007/s11356-022-21477-3>

- Kurokawa J, Ohara T (2020) Long-term historical trends in air pollutant emissions in Asia: Regional Emission inventory in ASia (REAS) version 3. *Atmos. Chem. Phys* 20:12761–12793
- Kwiatkowski L, Torres O, Bopp L, Aumont O, Chamberlain M, Christian JR, Dunne JP, Gehlen M, Ilyina T, John JG, Lenton A (2020) Twenty-first century ocean warming, acidification, deoxygenation, and upper-ocean nutrient and primary production decline from CMIP6 model projections. *Biogeosciences* 17(13):3439–3470
- Lachkar Z, Levy M, Smith S (2019) Strong intensification of the Arabian Sea oxygen minimum zone in response to Arabian Gulf warming. *Geophys. Res. Lettrs* 46:5420–5429
- Leon JF, Legrand M (2003) Mineral dust sources in the surroundings of the North Indian Ocean. *Geophys. Res. Lett* 30(42-1):42–44
- Li F, Ramanathan V (2002) Winter to summer monsoon variation of aerosol optical depth over the tropical Indian Ocean. *J. Geophys. Res. Atmos* 107(D16):AAC 2
- Löscher CR (2021) Reviews and syntheses: trends in primary production in the Bay of Bengal—is it at a tipping point? *Biogeosciences* 18(17):4953–4963
- Lozan JL, Grabl H, Hupfer P (2001) Summary: warning signals from climate. In: *Climate of 21st century: changes and risks*. Wissenschaftliche Auswertungen, Berlin, Germany, pp 400–408
- Mahowald N, Ward DS, Kloster S, Flanner MG, Heald CL, Heavens NG, Hess PG, Lamarque JF, Chuang PY (2011) Aerosol impacts on climate and biogeochemistry. *Annu Rev Environ Resour* 36:45–74
- Morel F, Rueter JG, Price NM (1991) Iron nutrition of phytoplankton and its possible importance in the ecology of ocean regions with high nutrient and low biomass. *Oceanogr* 4:56–61
- Nair SK, Parameswaran K, Rajeev K (2005) Seven-years satellite observations of the man structure and variabilities in the regional aerosol distribution over the oceanic areas around the Indian subcontinent. *Ann. Geophys* 23:2011–2030
- Narayanan Nampoothiri SV, Sachin TS, Rasheed K (2020) Dynamics and forcing mechanisms of upwelling along the south eastern Arabian sea during south west monsoon. *Reg. Stud. Mar. Sci* 40:101519
- Oschlies A, Brandt P, Stramma L, Schmidt S (2018) Drivers and mechanisms of ocean deoxygenation. *Nat. Geosci* 11(7):467–473
- Patra PK, Kumar MD, Mahowald N, Sarma VVSS (2007) Atmospheric deposition and surface stratification as controls of contrasting chlorophyll abundance in the North Indian Ocean. *J. Geophys. Res. Ocean* 112:C05029. <https://doi.org/10.1029/2006JC003885>
- Paul S (2018) A study on the impact of climatic events induced long-term trends in sea surface temperature and Ganges-Brahmaputra River discharge on the frequency and intensity of tropical cyclones over the Bay of Bengal, PhD Thesis., Andhra University
- Pease PP, Tchakerian VP, Tindale NW (1998) Aerosols over the Arabian Sea: geochemistry and source areas for aeolian desert dust. *J. Arid Environ* 39:477–496
- Poloczanska ES, Brown CJ, Sydeman WJ, Kiessling W, Schoeman DS, Moore PJ, Brander K, Bruno JF, Buckley LB, Burrows MT, Duarte CM (2013) Global imprint of climate change on marine life. *Nat Clim Chang* 3(10):919–925
- Pond S, Pickard GL (1983) *Introductory Dynamical Oceanography*, Second edn. Pergamon Press, Oxford
- Prakash P, Prakash S, Rahaman H, Ravichandran M, Nayak S (2012) Is the trend in chlorophyll-a in the Arabian Sea decreasing? *Geophys. Res. Lett* 39(23):n/a–n/a
- Prasanna Kumar S, Roshin RP, Narvekar J, Dinesh Kumar PK, Vivekanandan E (2010) What drives the increased phytoplankton biomass in the Arabian Sea? *Curr. Sci* 99:101–116
- Ramanathan V, Crutzen PJ, Lelieveld J, Mitra AP, Althausen D, Anderson J, Andreae MO, Cantrell W, Cass GR, Chung CE, Clarke AD (2001) Indian Ocean experiment: an integrated analysis of the climate forcing and effects of the great Indo-Asian haze. *J. Geophys. Res. Atmos* 106(D22):28371–28398
- Rao DN, Ghosh VRD, Sam P, Yadav K, Sarma VVSS (2021) Phosphate removal through adsorption on suspended matter in the Bay of Bengal: possible implications to primary production. *J. Earth Syst. Sci* 130(1):1–16
- Roxy MK, Ritika K, Terray P, Masson S (2015) Indian Ocean warming-the bigger picture. *Bull Am Meteorol Soc* 96(7):1070–1072
- Roxy MK, Modi A, Murtugudde R, Valsala V, Panickal S, Prasanna Kumar S, Ravichandran M, Vichi M, Lévy M (2016) A reduction in marine primary productivity driven by rapid warming over the tropical Indian Ocean. *Geophys. Res. Lett* 43(2):826–833
- Samsat BH, Sand M, Smith CJ, Bauer SE, Forster PM, Fuglestedt JS, Osprey S, Schleussner CF (2018) Climate impacts from a removal of anthropogenic aerosol emissions. *Geophys. Res. Lettrs* 45:1020–1029
- Santer BD, Wigley TML, Boyle JS, Gaffen DJ, Nychka D, Parker DE, Taylor KE (2000) Statistical significance of trends and trend differences in layer-average atmospheric temperature time series. *J. Geophys. Res. Atmos* 105:7337–7356
- Sarma VVSS, Sridevi B, Maneesha K, Sridevi T, Naidu SA, Prasad VR, Venkataramana V, Acharya T, Bharati MD, Subbaiah CV, Kiran BS (2013) Impact of atmospheric and physical forcings on biogeochemical cycling of dissolved oxygen and nutrients in the coastal Bay of Bengal. *J. Oceanogr* 69(2):229–243
- Sarma VVSS, Paul YS, Vani DG, Murty VSN (2015) Impact of river discharge on the coastal water pH and pCO₂ levels during the Indian Ocean Dipole (IOD) years in the western Bay of Bengal. *Cont. Shelf Res* 107:132–140
- Sarma VVSS, Rao GD, Viswanadham R, Sherin CK, Salisbury J, Omand MM, Mahedevan A, Murty VSN, Shroyer EL, Baumgartner M, Stafford KM (2016) Effects of freshwater stratification on nutrients, dissolved oxygen and phytoplankton in the Bay of Bengal. *Oceanogr* 29(2):222–231
- Sarma VVSS, Rao DN, Rajula GR, Dalabehera HB, Yadav K (2019) Organic nutrients support high primary production in the Bay of Bengal. *Geophys. Res. Lettrs* 46:6706–6715
- Sarma VVSS, Udaya Bhaskar TVS, Kumar JP, Chakraborty K (2020a) Potential mechanisms responsible for occurrence of core oxygen minimum zone in the north-eastern Arabian Sea. *Deep Sea Res. Part I Oceanogr. Res. Pap* 165:103393
- Sarma VVSS, Chopra M, Rao DN, Priya MMR, Rajula GR, Lakshmi DSR, Rao VD (2020b) Role of eddies on controlling total and size-fractionated primary production in the Bay of Bengal. *Cont. Shelf Res* 204:104186
- Sarma VVSS, Vivek R, Rao DN, Ghosh VRD (2020c) Severe phosphate limitation on nitrogen fixation in the Bay of Bengal. *Cont. Shelf Res* 205:104199
- Sarma VVSS, Sridevi B, Kumar A, Bikkina S, Kumari VR, Bikkina P, Yadav K, Rao VD (2022) Impact of atmospheric anthropogenic nitrogen on new production in the northern Indian Ocean: constrained based on satellite aerosol optical depth and particulate nitrogen levels. *Environ Sci Process Impacts* 24:1895
- Satheesh SK, Srinivasan J (2002) Enhanced aerosol loading over Arabian Sea during the pre-monsoon season: Natural or anthropogenic? *Geophys. Res. Lett* 29(18):21
- Schoffman H, Lis H, Shaked Y, Keren N (2016) Iron–nutrient interactions within phytoplankton. *Front. Plant Sci* 7:1223
- Schott FA, McCreary JP Jr (2001) The monsoon circulation of the Indian Ocean. *Progress in Oceanography* 51(1):1–123
- Séférian R, Berthet S, Yool A, Palmieri J, Bopp L, Tagliabue A, Kwiatkowski L, Aumont O, Christian J, Dunne J, Gehlen M (2020) Tracking improvement in simulated marine biogeochemistry between CMIP5 and CMIP6. *Current Climate Change Reports*, pp 1–25

- Shafeeque M, Sathyendranath S, George G, Balchand AN, Platt T (2017) Comparison of seasonal cycles of phytoplankton chlorophyll, aerosols, winds and sea surface temperature off Somalia. *Front. Mar. Sci* 4:386. <https://doi.org/10.3389/fmars.2017.00386>
- Smirnov A, Holben BN, Eck TF, Dubovik O, Slutsker I (2003) Effect of wind speed on columnar aerosol optical properties at Mid-way Island. *J. Geophys. Res* 108:4802. <https://doi.org/10.1029/2003JD003879>
- Spielhagen RF, Wener K, Sorensen SA, Zamelczyk K, Kandiano E, Budeus G, Husum K, Marchitto TM, Hald M (2011) Enhanced modern heat transfer to the Arctic by warm Atlantic Water. *Science* 331:450–453
- Sridevi B, Sarma VVSS (2021) Role of river discharge and warming on ocean acidification and pCO₂ levels in the Bay of Bengal. *ellus B Chem Phys Meteoro* 73:1–20
- Srinivas B, Sarin MM (2013) Atmospheric deposition of N, P and Fe to the Northern Indian Ocean: implications to C-and N-fixation. *Sci. Total Environ* 456:104–114
- Srinivas B, Sarin MM, Kumar A (2011) Impact of anthropogenic sources on aerosol iron solubility over the Bay of Bengal and the Arabian Sea. *Biogeochemistry* 110(1-3):257–268. <https://doi.org/10.1007/s10533-011-9680-1>
- Stramma L, Johnson GC, Sprintall J, Mohrholz V (2008) Expanding oxygen-minimum zones in the tropical oceans. *science* 320(5876):655–658
- Trott CB, Subrahmanyam B, Murty VSN, Shriver JF (2019) Large-scale fresh and salt water exchanges in the Indian Ocean. *J. Geophys. Res* 124(8):6252–6269
- Udaya Bhaskar TV, Sarma VVSS, Pavan Kumar J (2021) Potential mechanisms responsible for spatial variability in intensity and thickness of oxygen minimum zone in the Bay of Bengal. *J. Geophys. Res. Biogeosciences* 126:e2021JG006341
- Westberry T, Behrenfeld MJ, Siegel DA, Boss E (2008) Carbon-based primary productivity modeling with vertically resolved photoacclimation. *Global Biogeochemical Cycles* 22(2):n/a–n/a
- Winn CD, Campbell L, Christian JR, Letelier RM, Hebel V, Dore JE, Fujieki L, Karl DM (1995) Seasonal variability in the phytoplankton community of the North Pacific Subtropical Gyre. *Glob. Biogeochem. Cycles* 9:605–620
- Yadav K, Sarma VVSS, Rao DB, Kumar MD (2016) Influence of atmospheric dry deposition of inorganic nutrients on phytoplankton biomass in the coastal Bay of Bengal. *Mar. Chem* 187:25–34
- Yadav K, Rao VD, Sridevi B, Sarma VVSS (2021) Decadal variations in natural and anthropogenic aerosol optical depth over the Bay of Bengal: influence of pollutants from Indo-Gangetic Plain. *Environ. Sci. Pollut. Res* 28:55202–55219
- Zhang J, Reid JS (2010) A decadal regional and global trend analysis of the aerosol optical depth using a data-assimilation grade over-water MODIS and Level 2 MISR aerosol products. *Atmos. Chem. Phys* 10(22):10949–10963
- Zhu A, Ramanathan V, Li F, Kim D (2007) Dust plumes over the Pacific, Indian and Atlantic oceans: climatology and radiative impact. *J. Geophys. Res. Atmos* 112:D16208. <https://doi.org/10.1029/2007JD008427>

Publisher's note Springer Nature remains neutral with regard to jurisdictional claims in published maps and institutional affiliations.

Springer Nature or its licensor (e.g. a society or other partner) holds exclusive rights to this article under a publishing agreement with the author(s) or other rightsholder(s); author self-archiving of the accepted manuscript version of this article is solely governed by the terms of such publishing agreement and applicable law.